



# **FACULTY OF ELECTRICAL ENGINEERING CTU IN PRAGUE**

**BACHELOR THESIS**

Timur Abragimovich

## **Utilization of DKI-MRI in patients with pharmacoresistant epilepsy due to focal cortical dysplasia**

Department of Circuit Theory

Supervisor of the bachelor thesis: prof. MUDr. Jakub Otáhal

Study programme: Medical Electronics and  
Bioinformatics

Prague 2024





## I. Personal and study details

Student's name: **Abragimovich Timur** Personal ID number: **507344**  
Faculty / Institute: **Faculty of Electrical Engineering**  
Department / Institute: **Department of Circuit Theory**  
Study program: **Medical Electronics and Bioinformatics**

## II. Bachelor's thesis details

Bachelor's thesis title in English:

**Utilization of DKI-MRI in patients with pharmaco-resistant epilepsy due to focal cortical dysplasia**

Bachelor's thesis title in Czech:

**Využití DKI - MRI u pacientů s farmakorezistentní epilepsií na podkladě fokální kortikální dysplázie**

Guidelines:

1. Study the literature on the use of DKI MRI in the treatment of patients with FCD epilepsy and compile a comprehensive review.
2. Explore possible approaches for the selection of appropriate region of interest in the contralateral healthy hemisphere and propose the most suitable one.
3. On a given dataset, compare DKI metrics of epileptic lesions with the contralateral healthy brain regions in FCD patients.
4. Perform group comparison of DKI metrics in epileptic lesions in FCD patients versus in healthy controls
5. Discuss the potential applications of DKI metrics in the diagnosis and treatment of FCD patients and the potential application of advanced computer analysis in this task

Bibliography / sources:

Tabesh, A. et al. (2011) 'Estimation of tensors and tensor-derived measures in diffusional kurtosis imaging', *Magnetic Resonance in Medicine*, 65(3), pp. 823–836. doi: 10.1002/mrm.22655.  
Lu, H. et al. (2006) 'Three-dimensional characterization of non-gaussian water diffusion in humans using diffusion kurtosis imaging', *NMR in Biomedicine*, 19(2), pp. 236–247. doi: 10.1002/nbm.1020.

Name and workplace of bachelor's thesis supervisor:

**doc. MUDr. Jakub Otáhal, Ph.D. UK**

Name and workplace of second bachelor's thesis supervisor or consultant:

Date of bachelor's thesis assignment: **06.02.2024** Deadline for bachelor thesis submission: **24.05.2024**

Assignment valid until: **21.09.2025**

doc. MUDr. Jakub Otáhal, Ph.D.  
Supervisor's signature

doc. Ing. Radoslav Bortel, Ph.D.  
Head of department's signature

prof. Mgr. Petr Páta, Ph.D.  
Dean's signature

## III. Assignment receipt

The student acknowledges that the bachelor's thesis is an individual work. The student must produce his thesis without the assistance of others, with the exception of provided consultations. Within the bachelor's thesis, the author must state the names of consultants and include a list of references.

\_\_\_\_\_  
Date of assignment receipt

\_\_\_\_\_  
Student's signature

# Declaration

I declare that I elaborated this thesis on my own and that I mentioned all the information sources and literature that have been used in accordance with the Guideline for adhering to ethical principles in the course of elaborating an academic final thesis.

In Prague on May 23, 2024



# Dedication

With gratitude, I dedicated this work to my supervisor, prof. MUDr. Jakub Otáhal, Ph.D., and my academic advisor, Ing. David Kala, Ph.D., for their invaluable guidance. Many thanks also to the Czech Health Research Council for their funding support, grant number NU21-08-00228, which enabled the realization of this research. We would like to thank Veronika Borovcová and Jan Brhel for their exceptional skills as radiological assistants who play a crucial role in data acquisition.

Dedicated to my beloved wife, Katsiaryna, whose unwavering support and creative contributions in preparing certain figures have been priceless. And to the future free Belarus, a beacon of hope that lives in my heart.



# Abstract

This thesis investigates the distribution of diffusion kurtosis imaging (DKI) metrics in patients diagnosed with focal cortical dysplasia (FCD) types I and II, focusing particularly on those identified through structural T1 imaging. Utilizing multivariate statistical analysis, the study examines four DKI metrics (mean diffusivity, fractional anisotropy, mean kurtosis and kurtosis fractional anisotropy) concurrently, aiming to uncover novel combined metrics enhancing sensitivity for FCD-related differences. Results indicate statistically significant differences in DKI metrics, with notable practical significance observed predominantly in FCD type II patients. A novel combined metric derived exclusively for FCD type II patients is proposed, facilitating the identification of complex diffusion relationships in a multivariate context. This study sheds light on the potential of multivariate analysis in clarifying DKI metrics differences in FCD patients.

**Key words:** DKI, MRI, epilepsy, focal cortical dysplasia, multivariate analysis

# Abstrakt

Práce se zabývá distribucí metrik negaussovské difuze (diffusion kurtosis imaging; DKI) u pacientů s fokální kortikální dysplázií (FCD) typu I a II. Konkrétně pak v místech identifikovaných jako lesionální pomocí strukturálního T1 MRI. S využitím vícerozměrné statistické analýzy jsme zkoumali 4 metriky DKI (střední difuzivita, frakční anizotropie, střední kurtóza a kurtózní frakční anizotropie). Zároveň bylo cíleno na vytvoření nové, kombinované metriky, citlivější na difuzní rozdíly související s FCD. Výsledky ukazují statisticky významné rozdíly v metrikách DKI, přičemž největší praktická významnost byla pozorována převážně u pacientů s FCD typu II. Nová kombinovaná metrika odvozená pro pacienty s FCD typu II usnadňuje identifikaci komplexních funkcí difúzních stavů v multivariačním kontextu. Výsledky práce demonstrují potenciál vícerozměrné analýzy k objasnění rozdílů DKI metrik u pacientů s FCD.

**Klíčová slova:** DKI, MRI, epilepsie, fokální kortikální dysplázie, multivari-  
antní analýza



# Contents

<b>1</b>	<b>Introduction</b>	<b>5</b>
1.1	Epilepsy . . . . .	5
1.2	Focal Cortical Dysplasia (FCD) . . . . .	5
1.3	Preoperative Lesion Identification Using Structural MRI . . . . .	5
1.4	Diffusion of molecules in FCD . . . . .	7
1.5	Diffusion MRI . . . . .	8
1.5.1	Diffusion Tensor Imaging (DTI) . . . . .	8
1.5.2	Diffusion Kurtosis Imaging (DKI) . . . . .	10
1.5.3	Literature Overview: Use of Diffusion MRI in the epilepsy treatment . . . . .	10
1.6	Study Objectives . . . . .	11
1.6.1	Voxelwise Analysis . . . . .	12
1.6.2	Multivariate Contralateral Comparison Analysis . . . . .	12
1.6.3	Univariate Contralateral Analysis . . . . .	13
<b>2</b>	<b>Methods</b>	<b>15</b>
2.1	Dataset . . . . .	15
2.2	Lesions' T1 Segmentations and Brainmasking . . . . .	16
2.3	Contralateral Region Selection . . . . .	16
2.3.1	MNI Normalization . . . . .	16
2.3.2	Mirroring along the Sagittal Plane . . . . .	17
2.4	Voxelwise analysis . . . . .	17
2.4.1	Data preparation . . . . .	18
2.4.2	Canonical Correlation Analysis . . . . .	18
2.5	Contralateral Comparison . . . . .	19
2.5.1	Univariate Analysis . . . . .	19
2.5.2	Multivariate Analysis . . . . .	21
<b>3</b>	<b>Results</b>	<b>23</b>
3.1	Voxelwise Analysis . . . . .	23
3.1.1	Experimental group . . . . .	23
3.1.2	Control group . . . . .	25
3.2	Contralateral Comparison . . . . .	27
3.2.1	Multivariate Analysis . . . . .	27
3.2.2	Univariate Analysis . . . . .	33
<b>4</b>	<b>Discussion</b>	<b>43</b>
4.1	Statistical Analysis: Voxelwise and Contralateral Regions Comparison . . . . .	43
4.2	Univariate and Multivariate Contralateral Regions Comparison . . . . .	44
4.3	Contralateral Region Selection . . . . .	44
4.4	Application in Presurgical Diagnosis . . . . .	45
4.5	Advanced Image Processing Techniques . . . . .	46
4.5.1	Asymmetry Index . . . . .	46
4.5.2	Artificial Intelligence . . . . .	47

4.6 Future Work . . . . .	47
<b>5 Conclusion</b>	<b>49</b>
<b>List of Figures</b>	<b>55</b>
<b>List of Tables</b>	<b>57</b>
<b>List of Abbreviations</b>	<b>59</b>

# 1. Introduction

## 1.1 Epilepsy

Epilepsy is among the most prevalent neurological disorders globally, affecting approximately 50 million people worldwide.[1] One of the main symptoms is regular seizures, which are caused by excessive electrical activity of some neurons in the brain.[2]

Approximately 70% of patients can continue to live seizure-free with anti-seizure medications.[3] For the pharmaco-resistant, the next option that may help is to try to identify a single epileptic region, the so-called epileptic lesion, and surgically eliminate it. Today, to find this region, several both invasive and non-invasive examinations are carried out, such as EEG, PET, MRI, fMRI and others, each of which can indicate different boundaries of the lesion, as well as the type and likelihood of the absence of seizures after surgery. Therefore, it is important to continue research into various diagnostic methods, especially non-invasive ones, which can bring new information about the epileptic region of the region or reduce the need for invasive examinations, thereby increasing the accuracy of preoperative diagnosis.[4]

## 1.2 Focal Cortical Dysplasia (FCD)

One of the common causes of epilepsy is focal cortical dysplasia (FCD), which is a malformation of the brain cortex. FCD can be roughly divided into two types. FCD type I is often characterized by abnormal radial migration of neurons, while FCD type II is characterized by greater abnormalities and the presence of dysmorphic neurons.[5] As was said for epilepsy in general, FCD is also usually treated with medications, while for pharmaco-resistant the only causal therapy is resection of the lesion causing seizures.

## 1.3 Preoperative Lesion Identification Using Structural MRI

Resection is a surgical procedure with significant implications for the postoperative condition of the patient. Therefore, a detailed preoperative diagnosis is necessary to accurately identify the lesion. The goal is to adequately excise the affected region to mitigate or stop attacks while protecting against unnecessary injury to the patient as a result of excessive excision.[4]

One of the main examinations for preoperative localization of the lesion is MRI. Several sequences are carried out such as T1-weighted imaging, T2-weighted imaging and FLAIR (fluid-attenuated inversion recovery), which make it possible to identify structural pathologies of the brain. Examples of these metrics for different types of FCD are shown in Figure 1.1.[6]

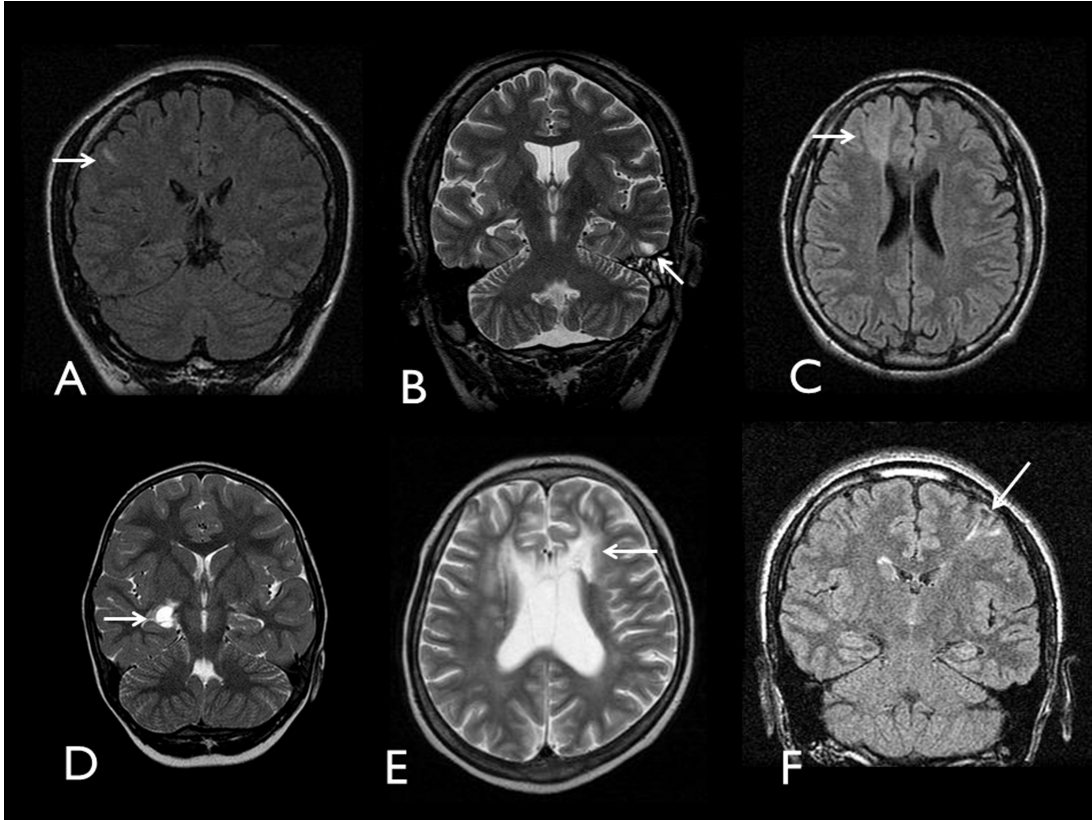


Figure 1.1: Illustrative MRI features in FCD patients. (A) Cortical high signal intensity on the FLAIR image in a patient with FCD IA; (B) mass-like lesion on the T2-weighted image in a patient with FCD IB; (C) cortical thickness, blurring of the gray–white matter junction, and subcortical high signal intensity (transmantle sign) on the FLAIR image in a patient with FCD IIB; (D) cyst-like lesion on the T2-weighted image in a patient with FCD IIIA (FCD with hippocampal sclerosis); (E) subcortical high signal intensity lesion on the T2-weighted image in a patient with FCD IIIC (FCD with angiomatosis); (F) cortical high signal intensity, cortical atrophy, and trauma-related scar on the FLAIR image in a patient with FCD IIID (FCD with traumatic lesion) FCD: focal cortical dysplasia, FLAIR: fluid-attenuated inversion recovery. Taken from [6]

It is worth noting that on MRI the lesion may often not be visible (especially typical for patients with FCD type I) or is visible smaller than it is. In some instances, certain lesions may only be discernible to a highly skilled radiologist with specialized expertise in the field. Conversely, there are occasions when an MRI scan might erroneously be considered negative. Therefore, we currently have to rely on other examinations even when abnormalities are found on MRI.[5] An example of a case where MRI was negative, but the lesion was detected using electroencephalography (EEG) and magnetoencephalography (MEG), is shown in Figure 1.2.[7]

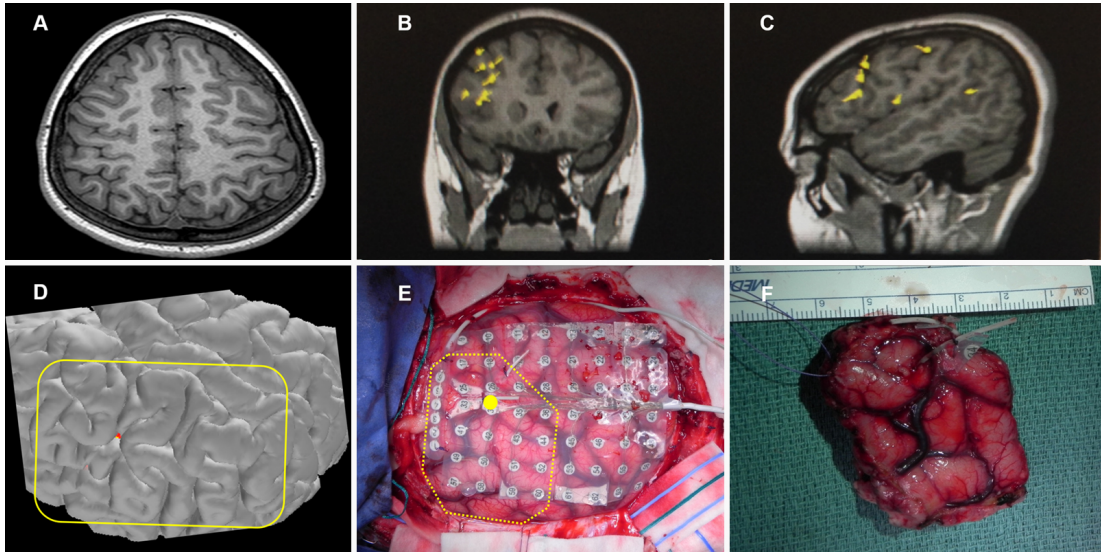


Figure 1.2: Presurgical evaluation with MEG and surgical findings. Preoperative axial T1-weighted image showing no observable abnormalities (A). The MEG findings were analyzed by the single-moving-dipole method (B and C; yellow circles with tails indicate the dipole source) and the AdSPM (D; red circle indicates the AdSPM spike source). Intraoperative resection planning (D and E; the yellow dotted line is the resection margin, and the yellow closed circle is the AdSPM spike source) and a photograph of the postresection specimen (F). Taken from [7]

## 1.4 Diffusion of molecules in FCD

As already noted, identifying the lesion area on structural MRI is challenging. Consequently, the lack of data in existing preoperative diagnostic examinations highlights the importance of exploring new methods to determine the area for resection.

An essential physiological parameter observable in the brain is the diffusion of molecules, particularly anisotropic diffusion. This process allows us to gain insight into the surrounding tissue and any potential abnormalities within it that may indicate various pathologies.[8]

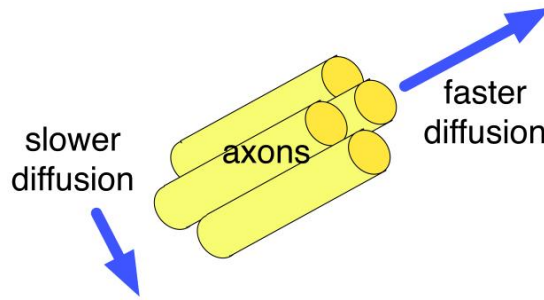


Figure 1.3: Schematic illustration describing the propagation of diffusion in axons. Taken from [9]

As for focal cortical dysplasia, the literature describes differences in the diffusion of extracellular spaces for this pathology. Histological examination showed significant differences for both patients with FCD type I and type II, but greater differences were observed in patients with FCD type II.[10]

## 1.5 Diffusion MRI

Until now, we focused exclusively on structural MRI images, which are predominantly used in modern medical practice. However, there are MRI sequences designed to provide physiological information about the brain. One such method is diffusion-weighted imaging (DWI).

To obtain a diffusion image, in addition to the standard main coil, which creates a powerful magnetic field, supplementary gradient coils are used (a simplified diagram is shown in Figure 1.4), which will send two pulses of a certain duration, amplitude and interval between them at the required time of the sequence. These pulses are characterized by  $b$ -value, which will be referenced in some equations throughout this work, although they are not central to the underlying understanding of this study.[11]

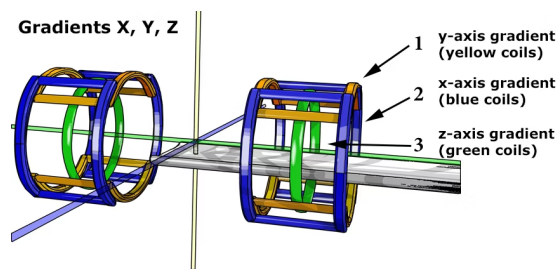


Figure 1.4: Simplified model describing coils in an MRI scanner. Taken from [12]

It is important to note that this method does not directly measure diffusion. Instead, it mathematically estimates the diffusion coefficient from Fick's law. Among these techniques, diffusion tensor imaging (DTI) and diffusion kurtosis imaging (DKI) are the most widely used.[13]

### 1.5.1 Diffusion Tensor Imaging (DTI)

When discussing anisotropic diffusion, it is important to consider its directional dependence, in contrast to isotropic diffusion in liquids, where measuring

the diffusion coefficient in one direction is sufficient. In diffusion tensor imaging (DTI), we solve this problem by characterizing diffusion at each point in space using a symmetric tensor

$$\mathbf{D} = \begin{pmatrix} D_{xx} & D_{xy} & D_{xz} \\ D_{xy} & D_{yy} & D_{yz} \\ D_{xz} & D_{yz} & D_{zz} \end{pmatrix}.$$

To construct it with DWI, it is necessary to calculate the diffusion coefficient in 6 directions, respectively using 6 different gradients.[14]

In DTI, it is assumed that particle diffusion adheres to a Gaussian distribution, so the diffusion coefficient  $D$  in a specific direction can be estimated from the sequence as:

$$S = S_0 \exp(-bD) \quad (1.1)$$

where:

$S$  - measured signal intensity at  $b \neq 0$

$S_0$  - measured signal intensity at  $b = 0$  (no gradient applied)

[11]

In practice, due to the multidimensional complexity, we do not use the tensor itself but rather the metrics derived from it, such as Mean Diffusivity (MD) and Fractional Anisotropy (FA).

### Mean Diffusivity (MD)

MD indicates the magnitude of the diffusion. In environments where diffusion occurs dynamically, such as fluid-rich environments like cerebral spinal fluid (CSF), MD tend to be high, resulting in lighter areas in the image. Conversely, darker areas in the image indicate less diffusion intensity.

MD can be computed using the eigenvalues  $\lambda_1, \lambda_2, \lambda_3$  of the diffusion tensor  $\mathbf{D}$ :

$$MD = \frac{\lambda_1 + \lambda_2 + \lambda_3}{3}. \quad (1.2)$$

[15]

### Fractional Anisotropy (FA)

The second important indicator is FA, which represents the anisotropy of ongoing diffusion. FA varies from 0 to 1: 0 indicates ideal isotropic diffusion, which occurs uniformly in all directions, and 1 denotes exclusively diffusion in one direction.

Fractional anisotropy can also be calculated using eigenvalues  $\lambda_1, \lambda_2, \lambda_3$

$$FA = \sqrt{\frac{3}{2} \cdot \frac{(\lambda_1 - MD)^2 + (\lambda_2 - MD)^2 + (\lambda_3 - MD)^2}{\lambda_1^2 + \lambda_2^2 + \lambda_3^2}} \quad (1.3)$$

[15]

## 1.5.2 Diffusion Kurtosis Imaging (DKI)

One limitation of DTI is the assumption that diffusion follows a Gaussian distribution, which is often not true in biological tissues. This limitation can be addressed by including kurtosis, which measures the "tailedness" of the distribution compared to the normal distribution. Figure 1.5 illustrates this concept.

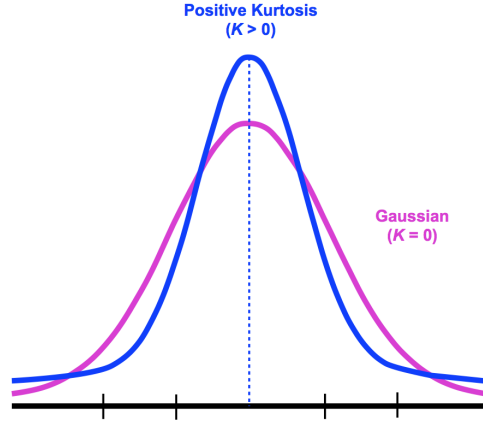


Figure 1.5: A graph explaining what kurtosis means in the sense of normal distribution. Taken from [16]

In the context of DKI, to describe diffusion, unlike DTI, not only the diffusion tensor  $\mathbf{D}$  is required, but also the calculation of the  $3 \times 3 \times 3 \times 3$  kurtosis tensor  $\mathbf{K}$ . In this case, to calculate the values of the tensors, the formula (1.1) is transformed to the form

$$S = S_0 \exp\left(-bD + \frac{1}{6}b^2D^2K\right) \quad (1.4)$$

where:

$S$  - measured signal intensity at  $b \neq 0$

$S_0$  - measured signal intensity at  $b = 0$  (no gradient applied)

[17]

Due to the symmetry of tensors, to construct them it is necessary to carry out a total of 21 measurements of at least two  $b$ -values other than zero.

From DKI, we can additionally derive two commonly used metrics: Kurtosis Fractional Anisotropy (KFA) and Mean Kurtosis (MK). MK and KFA have a similar interpretation in the sense of diffusion as MD and FA, but are calculated in a more complex way from the fourth-order kurtosis tensor  $\mathbf{K}$ , so we will not indicate these calculations in this work.[18]

## 1.5.3 Literature Overview: Use of Diffusion MRI in the epilepsy treatment

Diffusion MRI is known to detect white matter abnormalities more accurately than structural MRI, which has led to its consideration in preoperative diagnosis.[19] Numerous researchers around the world have reported an association between diffusion imaging and the presence of epilepsy in patients.

Several studies have shown that patients with epilepsy often exhibit increased mean diffusivity (MD), decreased fractional anisotropy (FA), and decreased mean kurtosis (MK).[19, 20] These changes are usually associated with myelin abnormalities, neuronal death, and diminished arborisation. However, there are also conflicting results, likely due to differences in methodology, types of epilepsy, and other factors. The exact reasons for these discrepancies remain unclear.[21]

Notably, the abnormalities detected by diffusion MRI were confirmed in patients whose structural MRI results were negative. Additionally, in patients with significant abnormalities on structural MRI, diffusion MRI provides even clearer visualization of the lesion compared to patients with negative MRI findings.[19]

Researchers have also successfully developed combined metrics based on MD, FA, and MK to improve the accuracy of lesion detection.[20] Several machine learning classifiers have demonstrated significant benefits from combining multiple metrics such as FA and MK.[22] One classifier that directly used the diffusion and kurtosis tensors achieved the best results, with the kurtosis tensor-based classification being particularly accurate (Area Under the Curve (hereinafter AUC) 0.99 compared to 0.96 for diffusion tensor imaging).[23]

Despite these advances, there are still limitations and gaps in the use of diffusion measures in clinical practice, such as:

- Uncertainty regarding whether the abnormalities observed on diffusion MRI are the initial cause of seizures or if they develop due to recurrent seizure activity.[5]
- Lack of multivariate statistical analysis, as most studies evaluate each metric separately, although Artificial Intelligence (AI) is starting to improve the combination of the two.
- Limited understanding of the relationship between diffusion measures and different types of focal cortical dysplasia (FCD). It is unclear which types of FCD and which diffusion parameters or combinations thereof are most significant for preoperative diagnosis and predicting surgical outcomes.
- The correlation between diffusion parameters and histological results remains under-researched.[24]

Overall, there is a need for more extensive studies examining different types of FCD, especially in patients with negative MRI findings. Diffusion MRI has the potential to significantly improve the accuracy of preoperative diagnosis and reduce the need for invasive and radioactive interventions, especially in these patients.

## 1.6 Study Objectives

Based on the introduction to the problem, the following objectives of this study were formulated:

- Determine the relationship between diffusion metrics and radiologist designation of voxels as lesions, elucidating the extent of their correlation. Ideally, we aim for as significant differences as possible between voxels from affected regions and healthy tissues.

- Ascertain disparities in diffusion distribution between the radiologist-identified lesion and contralateral healthy region. If possible, create a new metric as a combination of existing ones, which will be more effective in identifying epileptic lesions.
- Investigate variances in the distribution of individual diffusion metrics within the lesion compared to the contralateral healthy region. It is expected that there will be a practically significant difference in the distribution of the lesion compared to the contralateral region, making it easily discernible by the radiologist, either through individual diffuse metric alone or following monadic operation such as contrast enhancement.

We will analyze each of them and formulate suitable null hypotheses, to which the further text of the publication will be devoted.

### 1.6.1 Voxelwise Analysis

To determine how specific voxels from lesions are compared to healthy ones based on diffusion metrics, we can measure the correlation coefficient  $r$  between diffuse metrics and their designation as lesion. If there is no significant correlation with epilepsy, then the coefficient should be equal to the coefficient in the analysis of the control group, otherwise we can talk about a connection between diffusion and epilepsy voxelwise. Based on this, formulate a null hypothesis:

*$H_0^1$ : The correlation coefficient  $r$  of diffusion parameters and binary identification of voxels as affected is not significantly higher than in the control group.*

If the hypothesis holds, there is no significant difference in diffusion metrics for voxels of epilepsy-related lesions identified by radiologists.

### 1.6.2 Multivariate Contralateral Comparison Analysis

The upcoming objective is to elucidate whether diffusion parameters in the lesion vary from those in normal, as opposed to the previous step which focused solely on voxelwise comparison. However, the selection of a healthy region for such comparison is not a trivial task. Given the inherent heterogeneity of the brain, it is not sufficient to randomly select a proportionate healthy segment for comparison. In a healthy population, the closest analogue is usually the contralateral region due to partial symmetry of the brain. In this context, we consider a situation where we utilize all diffusion metrics in a four-dimensional space and compare these regions.

It is important to remember that the brain itself exhibits inherent asymmetry, so our focus lies not in discerning the mere presence of contralateral disparities, but rather in assessing the extent of such differences compared to the control group, where we expect contralateral disparities solely due to physiological asymmetry. To achieve this goal, we utilise correlation coefficients  $r$ , operating as the effect size when comparing the distributions of contralateral regions. A higher correlation coefficient signifies a more discernible difference between regions in practical terms. After comparing the distribution of the correlation coefficient  $r$

for the experimental group with the control group, we can determine the presence or absence of observable asymmetry associated with epilepsy. Based on this, formulate a null hypothesis:

*$H_0^2$ : There is no significant difference in the distribution of diffusion dissimilarities, as measured by the correlation coefficient  $r$ , between the radiologist-identified lesions and the healthy contralateral regions in both the experimental and control groups.*

If the hypothesis holds, it implies that any observed contralateral disparities are solely attributed to physiological asymmetry rather than epilepsy.

### 1.6.3 Univariate Contralateral Analysis

When formulating the previous hypothesis, we used all diffusion metrics in the assessment. Nowadays, doctors predominantly evaluate each parameter separately. Therefore, we construct an equivalent hypothesis to the previous one, but using each metric individually, i.e., univariately. The null hypothesis is formulated as follows:

*$H_0^3$ : There is no significant difference in the distribution of diffusion dissimilarities, as measured by the correlation coefficient  $r$ , between the radiologist-identified lesions and the healthy contralateral regions for individual diffusion metric in both the experimental and control groups.*

If the hypothesis holds, it implies that any observed contralateral disparities in individual diffusion metrics are solely attributed to physiological asymmetry rather than epilepsy.



## 2. Methods

### 2.1 Dataset

The dataset comprises 11 patients in the experimental group and 11 patients in the control group, all treated at Motol University Hospital for diagnosed FCD. Among the patients in the experimental group, there are 4 people with FCD type I, 5 patients with FCD type II and 2 patients with a different malformation of cortical development (MCD) than FCD. The experimental group consists of 5 males and 6 females, while the control group comprises 4 males and 7 females. The average MRI age of patients in the experimental group is 11.5 years (Standard Deviation  $SD = 15$ ), compared to 28 years ( $SD = 8$ ) in the control group. All patients with the specified diagnosis, as well as their age at MRI and sex, are listed in the table below.

	Patient	Diagnosis	Age at MRI	Sex
Experimental group	1706135	FCD type I	10	Male
	2075044	FCD type I	17	Female
	2100410	FCD type II	55	Male
	2133603	Different MCD than FCD	6	Female
	2135840	FCD type II	5	Female
	2141300	FCD type II	3	Female
	2212090	FCD type I	5	Female
	2218031	FCD type I	1	Male
	2252569	Different MCD than FCD	7	Male
	2258839	FCD type II	8	Female
	2301188	FCD type II	9	Male
Control group	C14.1706135	Normal	23	Female
	C15.2075044	Normal	24	Male
	C16.2100410	Normal	23	Male
	C17.2133603	Normal	25	Male
	C18.2135840	Normal	23	Male
	C19.2141300	Normal	40	Female
	C20.2212090	Normal	48	Female
	C21.2218031	Normal	31	Female
	C22.2252569	Normal	24	Female
	C23.2258839	Normal	23	Female
	C24.2301188	Normal	25	Female

Table 2.1: Patients of the control and experimental groups

All subjects signed an informed consent form and the study was approved by the Ethics Committee of the Motol University Hospital. This study was designed in accordance with the Declaration of Helsinki.

## 2.2 Lesions' T1 Segmentations and Brainmasking

For patients in the experimental group, the radiologist marked the border of the epileptic lesions using T1-weighted images, which we will subsequently use to assess the visibility of epilepsy manifestations using diffusion metrics.

We will also test patients in the control group using the same methods. Therefore, it is necessary to select comparable regions for them to those affected in the experimental group. To achieve this, we have randomly paired patients from both groups, ensuring each control patient has a designated region equivalent to that of their paired experimental group patient. The patient ID indicates the pairing: the number following the underscore "\_" corresponds to the corresponding patient from the experimental group.

When diagnosing epilepsy through diffusion parameters, we exclusively analyze diffusion in brain tissues such as white and grey matter, while isotropic fluids such as CSF do not carry any important information for this purpose. That's why in this study, all diffusion analysis was applied to the segmented brain without CSF. Segmentations of the white and grey were generated with the Computational Anatomy Toolbox for SPM[25].

## 2.3 Contralateral Region Selection

The step of selecting the contralateral region to the epileptogenic lesion is involved in the majority of the pipelines of this study. There is no single way to achieve this goal, and choosing a specific one is a compromise between ease of implementation, processing power, memory involved and accuracy for a particular case. The main method used in this study is based on the principle of normalizing the image to the MNI template for subsequent mirroring along the sagittal plane of the brain. This whole procedure is shown in diagram 2.1.

### 2.3.1 MNI Normalization

In many studies, we need to compare MRI images. Even within a single patient, different scans may show the brain in slightly different positions. This issue can be addressed by registering the images to register them, as the differences are typically due to variations in head positioning during the scans.

However, research often involves analyzing groups of patients rather than just individuals. Ideally, all anatomical regions of the brain should be in the same position across all images, regardless of differences in brain size, physiological variation, or other natural differences between patients. To achieve this, brain templates have been developed, and constructed from multiple brain images. One commonly used template is the MNI template. To align individual brain MRIs with the MNI template, nonlinear transformations are applied, ensuring that the resulting brain images conform as closely as possible to the "average" template brain.

To align with the MNI template for normalization, we use the SPM12 software. Table 2.2 outlines the configuration settings utilized for this purpose. The

transformation was derived from the T1 image and subsequently applied to MD, FA, MK, KFA, and lesion segmentation.

Setting	Option
Bias Regularization	0.0001
Bias FWHM	60
Tissue probability map	spm12 TPM
Affine Regularization	mni
Warping Regularisation	[0 0.001 0.5 0.05 0.2]
Smoothness	0
Sampling Distance	3
Bounding Box	[-78 -112 -70; 78 76 85]
Voxel Size	[1 1 1]
Interpolation Method	Nearest Neighbor

Table 2.2: Configuration Settings for MNI Normalization

### 2.3.2 Mirroring along the Sagittal Plane

After normalization to MNI, we can use the characteristic that the sagittal plane coincides with the  $yz$ -plane in MNI space, and therefore for mirroring it will be enough to replace the  $x$ -coordinate of each voxel with the opposite value, meaning to apply the transformation defined by the following matrix

$$\begin{pmatrix} -1 & 0 & 0 \\ 0 & 1 & 0 \\ 0 & 0 & 1 \end{pmatrix}.$$

to the position of each voxel.

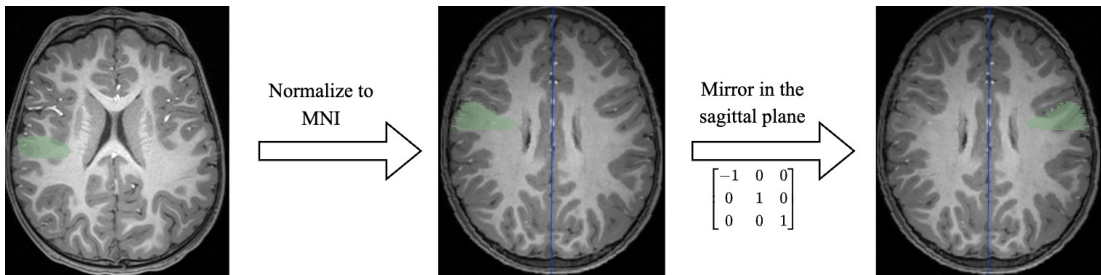


Figure 2.1: Diagram: Mirroring in MNI space

## 2.4 Voxelwise analysis

The first step in assessing the utility of diffuse metrics in preoperative diagnosis is determining whether specific diseases can be identified through individual voxels on diffusion MRI. In this study, we approach this by identifying a linear subspace within the space of all diffusion metrics (MD, FA, MK, KFA) where the intensity distributions of voxels marked as lesions by the radiologist differ significantly from those of healthy voxels. Essentially, we aim to test the null

hypothesis  $H_0^1$ : "The correlation coefficient  $r$  of diffusion parameters and binary identification of voxels as affected is not significantly higher than in the control group". This will help us identify the voxels that are most or least likely to be diseased. For our data analysis, we utilized canonical correlation analysis (CCA). The entire process is illustrated in Figure 2.2.

### 2.4.1 Data preparation

The diseased voxels were acquired from patients' labelled lesions in the experimental dataset. A limitation of this is that the relatively small number of patients results in a limited number of regions. Due to the brain's inhomogeneity, we can't claim that our sample sufficiently represents epilepsy-affected voxels for the entire population. Therefore, if we uniformly select healthy voxels from the entire brain, their distribution may differ not because they are from nonlesioned regions, but because they are generally from different brain regions not represented among radiologist-identified voxels. Healthy voxels were selected exclusively from the contralateral regions to avoid this bias.

The second significant factor is the variation in the sizes of lesions and their corresponding contralateral segments among different patients. When algorithms or statistical methods process the data, they treat each voxel as an individual data point. Therefore, regions with more voxels contribute more data points to the analysis. This numerical superiority means that the characteristics of larger regions are more heavily represented in the final results, potentially overshadowing the contributions from smaller regions. To reduce this factor, we will uniformly take only 2000 voxels from each region, which will allow voxels from smaller areas to have the same statistical impact as those from larger ones.

To assess the reliability of voxel reduction, we'll conduct the analysis ten times and compute both the mean and standard deviation for correlation coefficient  $r$ . Our expectation is for the standard deviation to be as small as possible, indicating that selecting voxels uniformly doesn't introduce significant errors in correlation measuring.

Finally, we performed  $Z$ -normalization along each axis. While CCA is inherently invariant to scaling, this step aids in interpreting the coefficients for each metric after CCA. These coefficients reflect the importance of the respective metrics in maximizing the correlation, as detailed in the next section.

### 2.4.2 Canonical Correlation Analysis

CCA is searching for linear combinations, meaning vectors  $a^T$  and  $b^T$ , of the random variables  $X$  and  $Y$  to maximize the correlation coefficient  $r$  between  $a^T X$  and  $b^T Y$ . In our case,  $X$  is represented as a matrix of voxel quaternities, taken after preprocessing as described in Section 2.4.1 above, where  $i$ -th is defined by values  $(MD_i, FA_i, MK_i, KFA_i)$ . While  $Y$  is represented as a 1D vector of labels with values "1" and "0", where "1" means that the voxel is from the epileptic lesion, and "0" is from the healthy region.

Through CCA processing, we will derive the canonical components, alongside their respective correlation coefficient  $r$ . By analyzing the coefficients of the linear combination for the component, we can determine which metrics (MD, FA,

MK, KFA) are qualitatively more suitable for FCD lesion detection. Quantitative comparison of these values is not advisable at this stage due to dataset size limitations. Nonetheless, we can consider the CCA component as an individual combined metric  $CM_{\text{voxelwise}}$ . Hypothetically, it could enhance FCD lesion detection by focusing exclusively on one metric rather than analysing each separately.

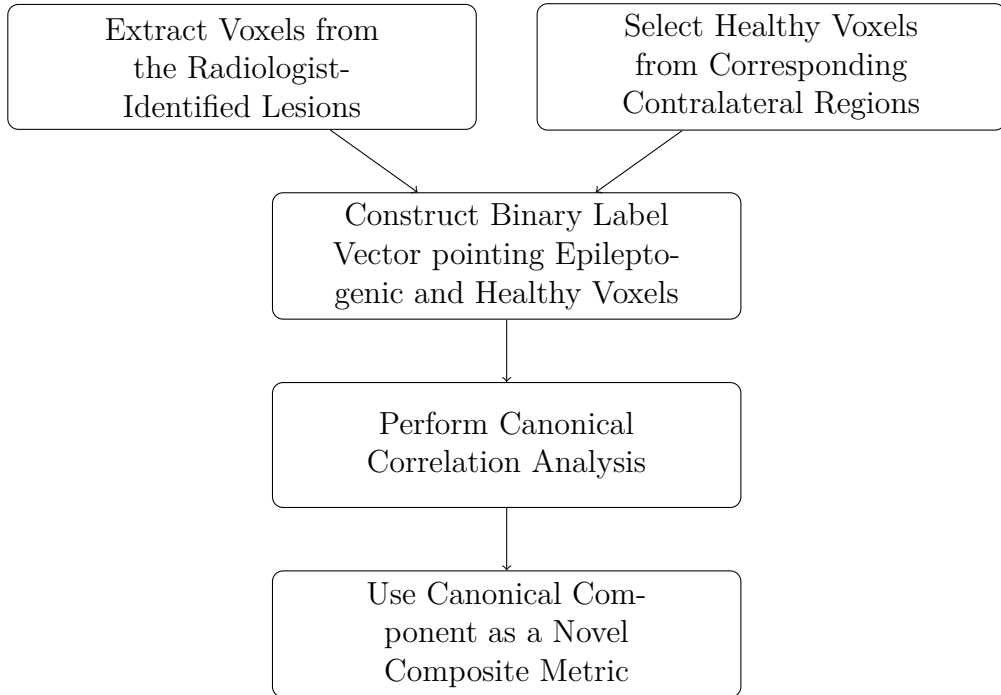


Figure 2.2: Voxelwise analysis pipeline Diagram

## 2.5 Contralateral Comparison

In the previous section, we compared FCD voxels of lesions with those of healthy regions, without considering their specific locations. At this stage, however, we compare the diffusion parameters of lesions with those of healthy regions for each patient individually. Due to the brain’s inherent heterogeneity, a randomly selected healthy segment is insufficient for comparison. The optimal reference in the healthy population is typically the contralateral region due to the partial symmetry of the brain.

### 2.5.1 Univariate Analysis

In univariate analysis, the goal is to identify differences between the lesion and the contralateral region for each metric individually.

#### Mann-Whitney U Test

One of the most common methods for univariate comparing distributions when a normal distribution cannot be assumed is the Mann-Whitney U test. The null hypothesis of this test states that two independent groups are homogeneous and have the same distribution.

However, it is worth noting that the  $p$ -value from the U test does not indicate the practical importance of the differences found in the distributions, but solely their statistical significance, since with a large number of samples the test can with great confidence reject the null hypothesis, finding the most insignificant differences in two distributions that have no practical impact.

### Correlation Coefficient $r$ as Effect Size

In voxelwise analysis, the coefficient  $r$  was used to measure the linear correlation between diffusion metrics and the binary category of voxels identified by the radiologist as lesioned. This approach can be similarly applied to contralateral analysis, with the key difference being that the voxels are derived from a single lesion and its contralateral region within the particular patient. However, to better understand and interpret the comparisons between regions rather than individual voxels, we can reformulate this interpretation. The correlation coefficient measures the degree of difference between voxels in two regions. Therefore, the correlation coefficient  $r$  can also be interpreted as an effect size, reflecting the difference between the probability distributions of subjects in the U test. This allows us to assess not only the statistical significance of the differences between the distributions but also their practical relevance. This implies that higher values of the correlation coefficient signify more significant practical disparities between distributions. For instance, Figure 2.3 illustrates this point, contrasting distribution histograms for correlation coefficients of 0.08 and 0.7. Notably, despite both U tests having a  $p$ -value  $< 0.001$ , the visual representation starkly underscores the difference in effect sizes.

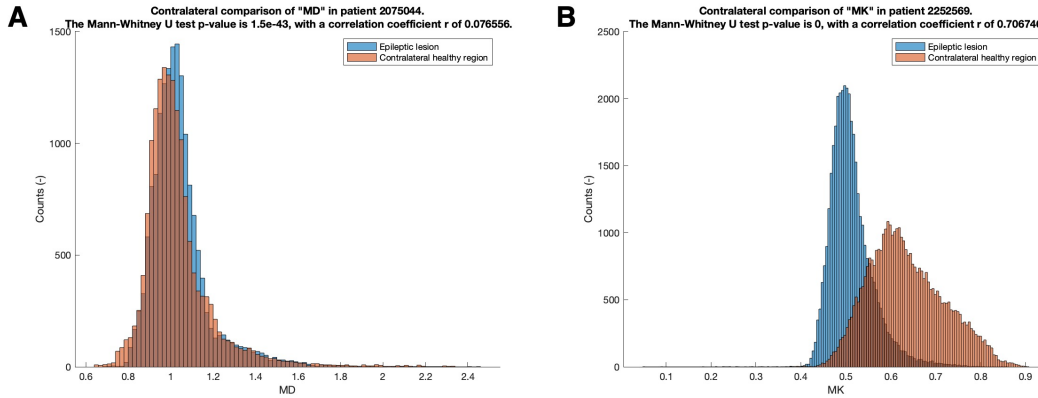


Figure 2.3: Visual representation of effect sizes contrasting correlation coefficients  $r$  of 0.08 (A) and 0.7 (B). In both scenarios, the U test yields a  $p$ -value less than 0.001

The correlation coefficient  $r$  from U statistics is defined as

$$r = \frac{Z}{\sqrt{n}} \tag{2.1}$$

where:

- $Z$  - standardized  $Z$ -score for the  $U$ -value
- $n$  - the total number of observations

[26]

It is worth noting that this correlation coefficient  $r$  differs from the previously mentioned Pearson correlation coefficient  $r$ . However, both have the same interpretation. Therefore, in the subsequent text, both will be referred to simply as the correlation coefficient  $r$  or just  $r$  without distinguishing between them. It is important to remember that these values cannot be numerically compared, only qualitatively.[26]

### Comparison with the Control Group

Subsequently, the obtained correlation coefficients  $r$  for the experimental group will be compared with the control group to statistically assess that the obtained differences between the lesion and the contralateral region are associated specifically with the manifestation of epilepsy, and not with physiological asymmetry of the brain. In other words, the objective is to either confirm or reject the hypothesis  $H_0^3$  "There is no significant difference in the distribution of diffusion dissimilarities, as measured by the correlation coefficient  $r$ , between the radiologist-identified lesions and the healthy contralateral regions for individual diffusion metric in both the experimental and control groups".

### 2.5.2 Multivariate Analysis

In multivariate analysis, similar to univariate analysis, the goal is to evaluate differences in lesion diffusion and contralateral region for a given patient, but using all diffusion metrics. Therefore, the issue is to compare distributions in a multidimensional space.

To assess how statistically different a lesion is from the contralateral one based on all four metrics together, we again use CCA as in Section 2.4.2, except for the correction of size in preprocessing, since the contralateral region for a particular patient has almost the same size. The correlation coefficient  $r$  is utilized to quantitatively assess differences in distributions across contralateral regions within the canonical component.

### Comparison with the Control Group

Subsequently, as in univariate analysis, the distribution of correlation coefficients  $r$  for the experimental group will be compared with the control group to ensure that the contralateral differences are not due to physiological asymmetry. In essence, the objective is to confirm or reject the null hypothesis  $H_0^2$  "There is no significant difference in the distribution of diffusion dissimilarities, as measured by the correlation coefficient  $r$ , between the radiologist-identified lesions and the healthy contralateral regions in both the experimental and control groups".

### Deriving a Combined Metric

The output coefficients of the linear combination for the canonical components were normalized with a vector norm of 1. Each can be represented as a unit direction vector describing a straight line in space. However, these lines can also be described by vectors symmetric to them, which complicates the selection process for comparing these coefficients with each other, since we do not know

exactly which of these vectors will be the result at the CCA output. Therefore, in each such pair, we iteratively select the one with the smallest angle from the previously selected one. This will allow us to compare these vectors and find a mean that will more sufficiently describe the canonical components in all patients. Subsequently, we will also take the mean value as a new combined metric  $CM_{\text{contralateral}}$ , which we will compare with the others in the univariate analysis described in Section 2.5.1.

It is worth noting that unlike the mean, which is a linear operation on vectors, we cannot calculate the standard deviation in a one-dimensional sense by figuring it out for each coordinate. To compute the dispersion of vectors, it is necessary to follow the principles of directional statistics with subsequent analysis of the covariance matrix, which will not be carried out in this work but can also be a useful step in further studies concerned with obtaining and comparing combined metrics for diffusion MRI.

# 3. Results

## 3.1 Voxelwise Analysis

In voxelwise analysis, the objective is to determine whether the voxels identified by the radiologist as lesions are distinct from those in healthy tissue. Specifically, we aim to test the null hypothesis  $H_0^1$  formulated in Section 1.6.1, which states: "The correlation coefficient  $r$  of diffusion parameters and binary identification of voxels as affected is not significantly higher than in the control group".

### 3.1.1 Experimental group

Voxelwise analysis was conducted ten times for the experimental group using CCA as detailed in Section 2.4. Table 3.1 presents the coefficients of the linear combination for the canonical component at each iteration, along with the corresponding correlation coefficient  $r$  values. Additionally, the mean coefficients were computed and are listed in the same table. By comparing the coefficients of a linear combination, we can observe which metrics influenced the most to maximize the correlation. The difference in probability distributions can also be evaluated through histograms for FCD lesioned and healthy voxels based on the mean component, as shown in Figure 3.1. Additionally, from the mean coefficients, a new combined metric  $CM_{\text{voxelwise}}$  was created, the effectiveness of which will subsequently be assessed in univariate analysis in Section 3.2.2:

$$CM_{\text{voxelwise}} = -0.1260 \cdot MD + 0.0677 \cdot FA + 0.9725 \cdot MK - 0.3533 \cdot KFA. \quad (3.1)$$

Iteration number	coeff. about MD	coeff. about FA	coeff. about MK	coeff. about KFA	$r$
1	-0.1255	0.0495	0.9804	-0.3586	0.2016
2	-0.1141	0.0462	0.9845	-0.3380	0.1952
3	-0.1321	0.0819	0.9657	-0.3572	0.1970
4	-0.1444	0.0614	0.9712	-0.3588	0.1945
5	-0.1001	0.0996	0.9646	-0.3514	0.1990
6	-0.1124	0.0509	0.9834	-0.3440	0.1918
7	-0.1450	0.0526	0.9753	-0.3567	0.1985
8	-0.1776	0.0461	0.9671	-0.3694	0.1980
9	-0.1249	0.0903	0.9628	-0.3557	0.1997
10	-0.0839	0.0984	0.9700	-0.3435	0.2003
Mean (SD)	-0.1260 (-)	0.0677 (-)	0.9725 (-)	-0.3533 (-)	0.1976 (0.0030)

Table 3.1: Results of voxelwise CCA with 10-fold repetition in experimental group patients with all FCD types. Larger absolute values of the coefficients for certain metrics indicate their significance in maximizing the correlation between healthy voxels and the radiologist selected as affected by epilepsy. Coefficient  $r$  indicates the degree of difference between distributions

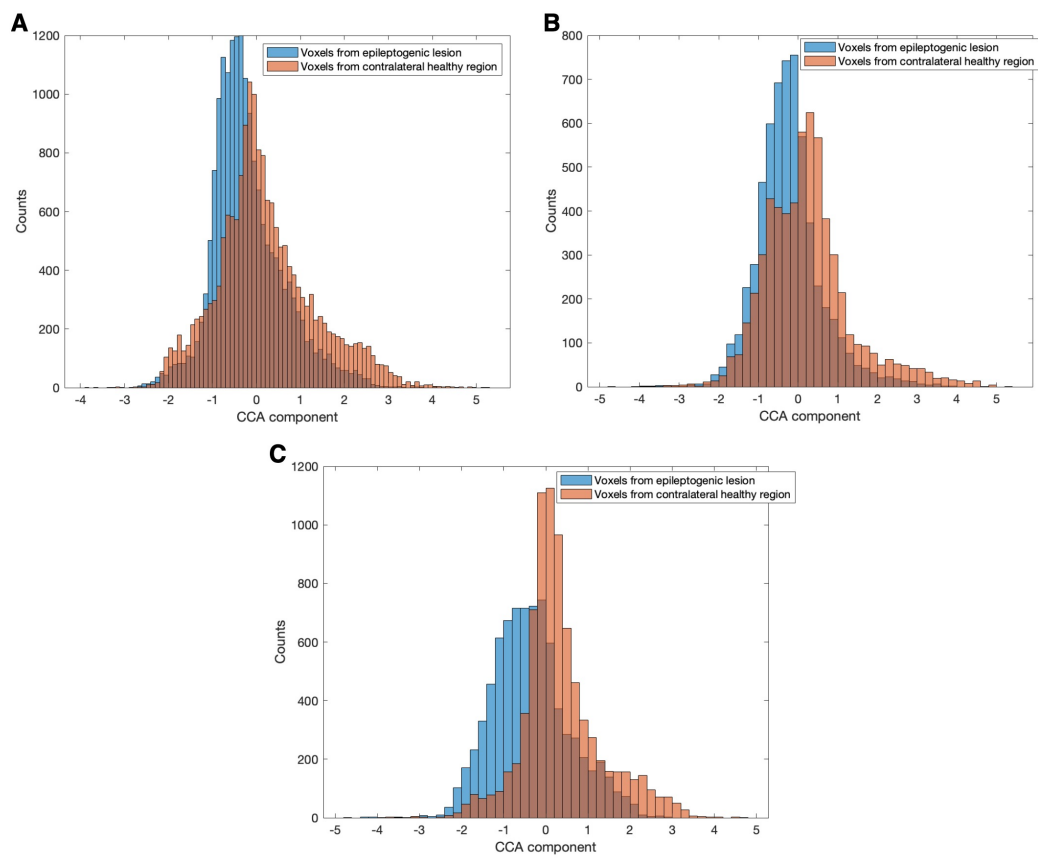


Figure 3.1: Histograms depict voxelwise disparities in the canonical component derived from the CCA. (A) showcases the canonical component across all patients, (B) and (C) illustrate the canonical components for patients with FCD types I and II, respectively

We also conducted separate analyses for patients diagnosed exclusively with FCD types I and II. The results are presented in Tables 3.2 and 3.3, respectively. Figure 3.1 also depicts histograms comparing the canonical components for each group of voxels. Notably, there is a higher correlation between voxels and their identification as lesions by radiologists in patients with FCD type II, with an  $r$  value of approximately 0.36, compared to 0.22 for patients with FCD type I. As in the analysis on all patients, combined metrics were created from the mean coefficients specifically for each FCD type, which will be considered together as  $CM_{\text{voxelwise (FCD specific)}}$  in the univariate analysis.

Iteration number	coeff. about MD	coeff. about FA	coeff. about MK	coeff. about KFA	$r$
1	-0.3041	0.0389	1.0966	-0.5977	0.2156
2	-0.3281	0.0606	1.0977	-0.6422	0.2279
3	-0.1933	0.0078	1.1289	-0.5576	0.2258
4	-0.1830	0.0239	1.1165	-0.5247	0.2265
5	-0.1975	0.1200	1.0760	-0.5765	0.2282
6	-0.2930	0.0279	1.1007	-0.5562	0.2142
7	-0.2657	0.0837	1.0815	-0.5503	0.2156
8	-0.3536	-0.0008	1.1185	-0.6489	0.2231
9	-0.1425	-0.0474	1.1505	-0.4783	0.2168
10	-0.3225	0.1055	1.0712	-0.5934	0.2153
Mean (SD)	-0.2583 (-)	0.0420 (-)	1.1038 (-)	-0.5726 (-)	0.2209 (0.0059)

Table 3.2: Results of voxelwise CCA with 10-fold repetition in experimental group patients with FCD type I. Larger absolute values of the coefficients for certain metrics indicate their significance in maximizing the correlation between healthy voxels and the radiologist selected as affected by epilepsy. Coefficient  $r$  indicates the degree of difference between distributions

### 3.1.2 Control group

To test the null hypothesis, we performed the same analysis on the control group. The correlation coefficient  $r$  for each iteration is presented in Table 3.4, with an average value of 0.0272. Using the Fisher transformation, we calculated the significance of the differences in the correlation coefficients between the experimental and control groups, as well as for each FCD type individually. The  $p$ -values for all tests were less than 0.001, leading us to reject the null hypothesis  $H_0^1$  for both FCD type I and FCD type II. Accordingly, we can argue that there is a significant correlation in diffusion metrics for voxels of epilepsy-related lesions identified by radiologists. Comparisons of correlation coefficients  $r$  among groups are shown in Figure 3.2.

Iteration number	coeff. about MD	coeff. about FA	coeff. about MK	coeff. about KFA	$r$
1	-0.6335	-0.5770	1.0690	-0.4078	0.3536
2	-0.6514	-0.5394	1.0525	-0.4263	0.3639
3	-0.6457	-0.5549	1.0645	-0.4193	0.3624
4	-0.5916	-0.5428	1.0815	-0.3962	0.3619
5	-0.6224	-0.5742	1.0774	-0.4062	0.3630
6	-0.6260	-0.5543	1.0668	-0.4047	0.3611
7	-0.6015	-0.5065	1.0640	-0.4142	0.3576
8	-0.6411	-0.5603	1.0660	-0.4163	0.3607
9	-0.6033	-0.5510	1.0822	-0.4024	0.3597
10	-0.5936	-0.5475	1.0800	-0.3869	0.3623
Mean (SD)	-0.6210 (-)	-0.5508 (-)	1.0704 (-)	-0.4080 (-)	0.3606 (0.0030)

Table 3.3: Results of voxelwise CCA with 10-fold repetition in experimental group patients with FCD type II. Larger absolute values of the coefficients for certain metrics indicate their significance in maximizing the correlation between healthy voxels and the radiologist selected as affected by epilepsy. Coefficient  $r$  indicates the degree of difference between distributions

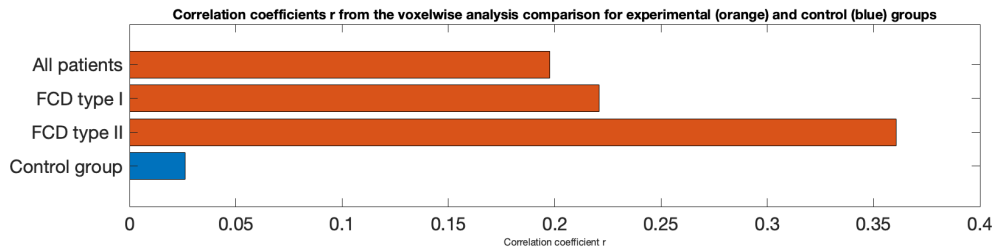


Figure 3.2: Comparisons of correlation coefficients  $r$  from the voxelwise analysis. A larger value of  $r$  means a greater correlation in diffusion metrics for voxels of epilepsy-related lesions identified by radiologists

Iteration	$r$
1	0.0227
2	0.0272
3	0.0224
4	0.0212
5	0.0280
6	0.0292
7	0.0282
8	0.0277
9	0.0278
10	0.0272
Mean (SD)	0.0262 (0.0029)

Table 3.4: Results of voxelwise CCA with 10-fold repetition in control group patients. Coefficient  $r$  indicates the degree of difference between distributions

## 3.2 Contralateral Comparison

### 3.2.1 Multivariate Analysis

#### MD & FA & MK & KFA

When performing contralateral analysis, we aim to analyse whether there are significant differences between the region identified by the radiologist as a lesion and its contralateral healthy region. We will measure the effect size of these differences using the correlation coefficient  $r$  for each patient, and subsequently, the same process will be conducted on a control group. The goal is to confirm or reject the null hypothesis  $H_0^2$ : "There is no significant difference in the distribution of diffusion dissimilarities, as measured by the correlation coefficient  $r$ , between the radiologist-identified lesions and the healthy contralateral regions in both the experimental and control groups". Accordingly, when obtaining larger values of the correlation coefficient  $r$  for the experimental group than for the control group, we can assert that there are significant practical contralateral differences associated with FCD and not physiological asymmetry of the brain.

Contralateral comparisons were performed using CCA for each patient separately as described in Section 2.5.2. The coefficients of the linear combination for each patient's canonical component, along with their mean, are documented in Table 3.5. For patient 2218031, the coefficients for the component were not recorded because the correlation coefficient  $r$  was very low (0.09).

patient	coeff. about MD	coeff. about FA	coeff. about MK	coeff. about KFA	$r$
2258839	-0.6899	-0.1992	0.5281	-0.4532	0.5775
2301188	0.0516	-0.6917	0.6371	-0.3362	0.4634
2252569	-0.2117	-0.3412	0.9059	-0.1347	0.7513
2212090	0.0337	-0.7310	0.4890	0.4748	0.6925
2135840	-0.6440	-0.1160	0.4466	-0.6102	0.5394
2100410	0.0552	-0.2730	0.6861	-0.6721	0.7546
2133603	-0.0625	-0.5059	0.6824	0.5240	0.8145
2141300	-0.0768	-0.5693	0.8083	-0.1290	0.6031
1706135	0.2820	-0.5799	0.1732	0.7445	0.4707
2075044	-0.4135	0.0973	0.6603	-0.6193	0.2829
2218031	-	-	-	-	0.0933
Mean (SD)	-0.1676 (-)	-0.3910 (-)	0.6017 (-)	-0.1212 (-)	0.5494 (0.2168)

Table 3.5: Results of multivariate analysis using CCA in all patients in the experimental group. Larger absolute values of the coefficients for certain metrics indicate their significance in maximizing the correlation (effect size of the dissimilarity in our case) between the radiologist-identified lesion and the contralateral healthy region

In the same way, an analysis was carried out exclusively for patients with FCD type I and FCD type II. The results are shown in Tables 3.6 and 3.7, respectively. As in voxelwise analysis, new combined metrics  $CM_{\text{contralateral}}$  were created from the coefficients of mean values, including for each FCD type separately.

Subsequently, a similar analysis was carried out on the control group. The results are recorded in Table 3.8. The distribution of correlation coefficients  $r$

patient	coeff. about MD	coeff. about FA	coeff. about MK	coeff. about KFA	$r$
2212090	0.0337	-0.7310	0.4890	0.4748	0.6925
1706135	0.2820	-0.5799	0.1732	0.7445	0.4707
2075044	0.4135	-0.0973	-0.6603	0.6193	0.2829
2218031	-	-	-	-	0.0933
Mean (SD)	0.2431 (-)	-0.4694 (-)	0.0006 (-)	0.6128 (-)	0.3848 (0.2565)

Table 3.6: Results of multivariate analysis using CCA in patients with FCD type I in the experimental group. Larger absolute values of the coefficients for certain metrics indicate their significance in maximizing the correlation (effect size of the dissimilarity in our case) between the radiologist-identified lesion and the contralateral healthy region

patient	coeff. about MD	coeff. about FA	coeff. about MK	coeff. about KFA	$r$
2258839	-0.6900	-0.1992	0.5281	-0.4532	0.5775
2301188	0.0516	-0.6917	0.6371	-0.3362	0.4634
2135840	-0.6440	-0.1160	0.4466	-0.6102	0.5394
2100410	0.0552	-0.2730	0.6861	-0.6721	0.7546
2141300	-0.0768	-0.5693	0.8083	-0.1290	0.6031
Mean (SD)	-0.2608 (-)	-0.3698 (-)	0.6212 (-)	-0.4401 (-)	0.5876 (0.1072)

Table 3.7: Results of multivariate analysis using CCA in patients with FCD type II in the experimental group. Larger absolute values of the coefficients for certain metrics indicate their significance in maximizing the correlation (effect size of the dissimilarity in our case) between the radiologist-identified lesion and the contralateral healthy region

between the experimental and control groups can be compared using boxplots in Figure 3.3. Using the Mann-Whitney U test, we evaluated the significance of distribution differences and obtained a  $p$ -value of 0.003 when comparing the experimental group to the control group. Furthermore, the correlation coefficients for patients with FCD type II significantly differed from the controls with a  $p$ -value  $< 0.001$ . In contrast, for patients with FCD type I, the  $p$ -value was 0.28. This indicates we could reject the null hypothesis  $H_0^2$  regarding contralateral differences in diffusion metrics with 99% confidence for patients with FCD type II. Therefore, given the higher correlation coefficient  $r$  values observed in patients with FCD type II compared to healthy controls, we can conclude that significant contralateral differences are visibly associated with this pathology. For 4 patients with FCD type I, the data did not allow us to confirm or deny the hypothesis significantly.

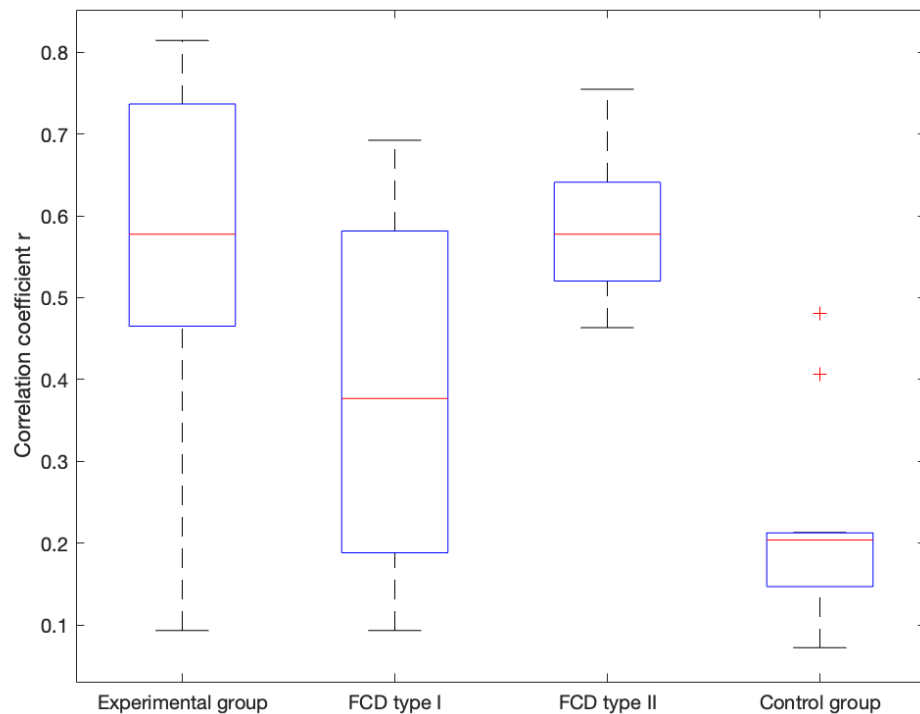


Figure 3.3: Distributions of correlation coefficients  $r$  from multivariate analysis for the experimental and control groups. Using the Mann-Whitney U-test, significant differences in correlation  $r$  distributions were found between the experimental and control groups ( $p = 0.003$ ). Patients with FCD type II showed significant differences compared to controls ( $p < 0.001$ ), while patients with FCD type I did not ( $p = 0.28$ )

patient	coeff. about MD	coeff. about FA	coeff. about MK	coeff. about KFA	$r$
C14_1706135	0.3129	0.7646	-0.5541	-0.1024	0.2131
C15_2075044	-0.2690	0.5568	-0.7129	-0.3306	0.2038
C16_2100410	-0.0797	0.6077	-0.7400	-0.2771	0.4809
C17_2133603	-0.1947	0.7475	-0.4352	-0.4626	0.1416
C18_2135840	-0.3047	0.5016	0.0056	-0.8096	0.2100
C19_2141300	-0.4808	0.4626	-0.0633	-0.7422	0.1061
C20_2212090	-0.1890	0.0876	0.4753	-0.8548	0.1624
C21_2218031	-	-	-	-	0.0722
C22_2252569	-0.0733	0.5765	0.6077	-0.5414	0.2111
C23_2258839	-0.3070	0.3722	0.1508	-0.8628	0.4061
C24_2301188	-0.2963	0.5402	-0.3802	-0.6898	0.1648
Mean (SD)	-0.1882 (-)	0.5217 (-)	-0.1646 (-)	-0.5673 (-)	0.2157 (0.1226)

Table 3.8: Results of multivariate analysis using CCA in control group patients

## FA & MK

After performing CCA we attempt to create a new combined metric, in the case of contralateral analysis, as the mean of the components for each patient. Notably, there was significant variation in the coefficients, particularly among patients with FCD type I, as shown in Table 3.6. Consequently, we repeated the analysis, focusing exclusively on two specific metrics. At this step, only FA and MK are involved. This pair was chosen based on the fact that when one of these metrics has less significance in the contralateral comparison for a particular patient, the other still has a fairly high coefficient value. Calculations were also carried out for all patients and each of the FCD types separately. The results are listed in tables 3.9, 3.10, 3.11, respectively.

patient	coeff. about FA	coeff. about MK	$r$
2258839	-0.6512	0.7589	0.2159
2301188	-0.8484	0.5294	0.4537
2252569	-0.4040	0.9148	0.7377
2212090	-0.5223	0.8527	0.6316
2135840	-0.2489	0.9685	0.4867
2100410	-0.7730	0.6344	0.7294
2133603	-0.0165	0.9999	0.7658
2141300	-0.6244	0.7811	0.6000
1706135	0.2098	0.9777	0.1212
2075044	-0.3549	0.9349	0.2544
Mean (SD)	-0.4234 (-)	0.8352 (-)	0.4996 (0.2343)

Table 3.9: Results of contralateral multivariate analysis by CCA, using exclusively FA and MK metrics, in all patients in the experimental group. Larger absolute values of the coefficients for certain metrics indicate their significance in maximizing the correlation (effect size of the dissimilarity in our case) between the radiologist-identified lesion and the contralateral healthy region

patient	coeff. about FA	coeff. about MK	$r$
2212090	-0.5223	0.8527	0.6316
1706135	0.2098	0.9777	0.1212
2075044	-0.3549	0.9349	0.2544
Mean (SD)	-0.2225 (-)	0.9218 (-)	0.3357 (0.2647)

Table 3.10: Results of contralateral multivariate analysis by CCA, using exclusively FA and MK metrics, in patients with FCD type I in the experimental group. Larger absolute values of the coefficients for certain metrics indicate their significance in maximizing the correlation (effect size of the dissimilarity in our case) between the radiologist-identified lesion and the contralateral healthy region

patient	coeff. about FA	coeff. about MK	$r$
2258839	-0.6512	0.7589	0.2159
2301188	-0.8484	0.5294	0.4537
2135840	-0.2489	0.9685	0.4867
2100410	-0.7730	0.6344	0.7294
2141300	-0.6244	0.7811	0.6000
Mean (SD)	-0.6292 (-)	0.7345 (-)	0.4971 (0.1908)

Table 3.11: Results of contralateral multivariate analysis by CCA, using exclusively FA and MK metrics, in patients with FCD type II in the experimental group. Larger absolute values of the coefficients for certain metrics indicate their significance in maximizing the correlation (effect size of the dissimilarity in our case) between the radiologist-identified lesion and the contralateral healthy region

## KFA & MK

Similarly, as in the previous section, we carried out the same analysis, but exclusively on KFA and MK metrics. These metrics were selected specifically for their relevance to the transition from Diffusion Tensor Imaging (DTI) to Diffusion Kurtosis Imaging (DKI). The results are shown in tables 3.12, 3.13, 3.14.

patient	coeff. about KFA	coeff. about MK	$r$
2258839	-0.6539	0.7566	0.1877
2301188	-0.8951	0.4460	0.4455
2252569	-0.3612	0.9325	0.7158
2212090	-0.3896	0.9210	0.5498
2135840	-0.2118	0.9773	0.4744
2100410	-0.8431	0.5377	0.7518
2133603	0.1228	0.9924	0.7713
2141300	-0.6159	0.7878	0.5659
1706135	-0.9941	-0.1084	0.2074
2075044	-0.3756	0.9268	0.2606
Mean (SD)	-0.5218 (-)	0.7170 (-)	0.4930 (0.2196)

Table 3.12: Results of contralateral multivariate analysis by CCA, using exclusively KFA and MK metrics, in all patients in the experimental group. Larger absolute values of the coefficients for certain metrics indicate their significance in maximizing the correlation (effect size of the dissimilarity in our case) between the radiologist-identified lesion and the contralateral healthy region

patient	coeff. about KFA	coeff. about MK	$r$
2212090	-0.3896	0.9210	0.5498
1706135	-0.9941	-0.1084	0.2074
2075044	-0.3756	0.9268	0.2606
Mean (SD)	-0.5865 (-)	0.5798 (-)	0.3393 (0.1843)

Table 3.13: Results of contralateral multivariate analysis by CCA, using exclusively KFA and MK metrics, in patients with FCD type I in the experimental group. Larger absolute values of the coefficients for certain metrics indicate their significance in maximizing the correlation (effect size of the dissimilarity in our case) between the radiologist-identified lesion and the contralateral healthy region

patient	coeff. about KFA	coeff. about MK	$r$
2258839	-0.6539	0.7566	0.1877
2301188	-0.8951	0.4460	0.4455
2135840	-0.2118	0.9773	0.4744
2100410	-0.8431	0.5377	0.7518
2141300	-0.6159	0.7878	0.5659
Mean (SD)	-0.6440 (-)	0.7011 (-)	0.4851 (0.2048)

Table 3.14: Results of contralateral multivariate analysis by CCA, using exclusively KFA and MK metrics, in patients with FCD type II in the experimental group. Larger absolute values of the coefficients for certain metrics indicate their significance in maximizing the correlation (effect size of the dissimilarity in our case) between the radiologist-identified lesion and the contralateral healthy region

### 3.2.2 Univariate Analysis

In the previous Section 3.2.1, we examined contralateral differences using all diffusion metrics, a method seldom used in practice due to the challenges radiologists face in interpreting highly dimensional data. Typically, each metric is considered separately, so we will also analyze the comparison of radiologist-identified lesions with their contralateral healthy regions for each metric individually. Similar to the previous section, the goal is to confirm or refute the null hypothesis  $H_0^3$ : "There is no significant difference in the distribution of diffusion dissimilarities, as measured by the correlation coefficient  $r$ , between the radiologist-identified lesions and the healthy contralateral regions for individual diffusion metric in both the experimental and control groups". This means that to confirm epilepsy-related practical differences in a particular diffusion metric between the radiologist-identified FCD lesion and its healthy contralateral region, it is necessary to obtain significantly higher correlation coefficients  $r$  for the experimental group, reflecting practical differences in the distribution of the two regions, than for the control group. We can also evaluate and compare the effectiveness of the combined metrics (CM) developed in Sections 3.1 and 3.2.1.

In the univariate analysis, we measured the correlation coefficient  $r$  calculated using Equation 2.1, which describes the effect size of the U test in distinguishing the radiologist-identified lesion from the healthy contralateral region for each metric. The results of correlation coefficients are shown in Table 3.15. We can also estimate the resulting distributions for the correlation coefficient for each metric, including each FCD type separately, using boxplots shown in Figure 3.4. To focus solely on the medians, we created an additional Figure 3.5 featuring a bar plot that displays the medians and their 95% confidence intervals, which were calculated using the bootstrap method.

For FCD type I patients, the differences are best visible on the MK, worst of all on the MD. New metrics obtained using various CCA analyses described above did not bring new profit for FCD I patients. Notably, in the case of  $CM_{\text{contralateral}}$  using only FA and MK in patients with FCD type I, the result was better than using all 4 metrics. We interpret that this is due to the large variation among patients with FCD type I in the choice of linear combination, which prevents finding a suitable one.

The differences in patients with FCD type II are best seen on the KFA. At the same time, in contrast to FCD type I, we see a certain benefit in the use of  $CM_{\text{contralateral}}$ . Especially, the metric that emerged from the contralateral analysis specifically from patients with FCD type II performs best, receiving the highest median value and the smallest variation.

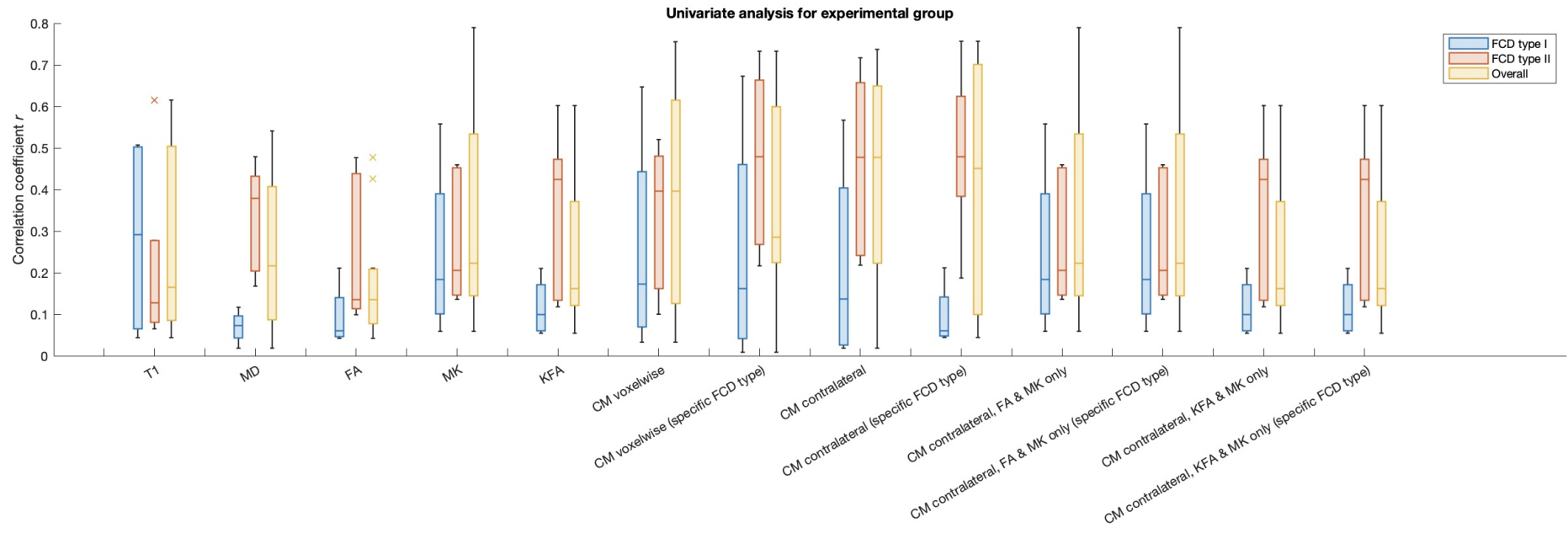


Figure 3.4: Box plots: Univariate analysis of the experimental group. A higher value of the correlation coefficient  $r$  indicates a greater practical discrepancy between the lesion and the contralateral healthy region

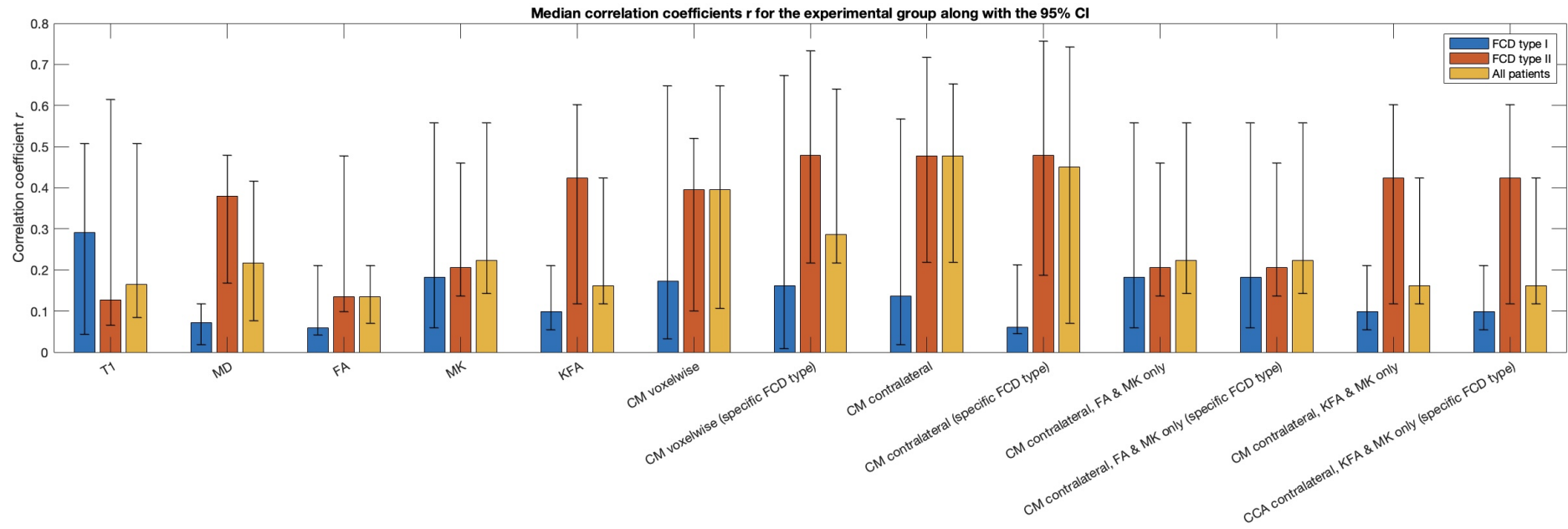


Figure 3.5: Bar plots: The medians of correlation coefficients  $r$  for the experimental group, along with their respective 95% confidence intervals (CI). A higher value of the correlation coefficient  $r$  indicates a greater practical discrepancy between the lesion and the contralateral healthy region

Metrics	Patients										
	2258839 (FCD2)	2301188 (FCD2)	2252569 (MCD)	2212090 (FCD1)	2135840 (FCD2)	2100410 (FCD2)	2133603 (MCD)	2218031 (FCD1)	2141300 (FCD2)	1706135 (FCD1)	2075044 (FCD1)
T1	0.0867	0.1650	0.2280	0.4970	0.6154	0.1270	0.5070	0.0436	0.0650	0.5070	0.0846
MD	0.4788	0.2164	0.3724	0.1168	0.3787	0.4162	0.5411	0.0182	0.1676	0.0684	0.0766
FA	0.1354	0.4263	0.2010	0.0423	0.0989	0.4766	0.1840	0.0702	0.1171	0.2109	0.0487
MK	0.1358	0.2055	0.7067	0.5577	0.4592	0.1502	0.7893	0.0592	0.4492	0.1429	0.2230
KFA	0.1393	0.4305	0.1991	0.1317	0.4241	0.6021	0.1617	0.0543	0.1179	0.2102	0.0669
CM <sub>voxelwise</sub>	0.1818	0.1009	0.7422	0.6464	0.4674	0.3938	0.7560	0.0332	0.5200	0.1066	0.2397
CM <sub>voxelwise</sub> (specific FCD type)	0.2133	0.0458	0.6841	0.6023	0.4740	0.5862	0.5891	0.0491	0.5841	0.1275	0.2319
CM <sub>contralateral</sub>	0.2179	0.2502	0.7370	0.5667	0.4781	0.7170	0.6521	0.0323	0.6376	0.0184	0.2399
CM <sub>contralateral</sub> (specific FCD type)	0.1870	0.4501	0.7419	0.0442	0.4786	0.7567	0.7564	0.0703	0.5803	0.2116	0.0496
CM <sub>contralateral</sub> , FA & MK only	0.1358	0.2055	0.7067	0.5577	0.4592	0.1502	0.7893	0.0592	0.4492	0.1429	0.2230
CM <sub>contralateral</sub> , FA & MK only (specific FCD type)	0.1358	0.2055	0.7067	0.5577	0.4592	0.1502	0.7893	0.0592	0.4492	0.1429	0.2230
CM <sub>contralateral</sub> , KFA & MK only	0.1393	0.4305	0.1991	0.1317	0.4241	0.6021	0.1617	0.0543	0.1179	0.2102	0.0669
CM <sub>contralateral</sub> , KFA & MK only (specific FCD type)	0.1393	0.4305	0.1991	0.1317	0.4241	0.6021	0.1617	0.0543	0.1179	0.2102	0.0669

Table 3.15: Correlation coefficients  $r$  for each metric across experimental group patients. A higher value of the correlation coefficient  $r$  indicates a greater practical discrepancy between the lesion and the contralateral healthy region

Notably, in patient 2100410, the contralateral differences in MK are significantly less pronounced than in MD, with a correlation coefficient of  $r = 0.15$  for MK compared to 0.42 for MD. Additionally, our multivariate analysis revealed that MK has a substantially greater influence on identifying the subspace with the maximum difference between distributions than MD, with a coefficient value of 0.68 for MK compared to 0.06 for MD. This finding suggests that MK’s significant contribution emerges when it is combined with other diffusion metrics, rather than being solely compared in isolation.

One more important finding is that the metrics on which we can best observe radiologist-identified lesions differ among some patients, even within the same FCD group. Such an example is depicted in Figure 3.6, where you can see how in one patient the contralateral differences between healthy region and lesion are better visible on MK (Figure 3.6A), and rather poorly on KFA (Figure 3.6B), while in the second patient, the situation is the opposite (Figures 3.6 D and E). But at the same time, both patients had a visible lesion on the new combined metric  $CM_{\text{contralateral}}$  calculated for patients with FCD type II (Figures 3.6 C and F). This result confirms the motivation for using a combination of several diffusion metrics to diagnose epilepsy.

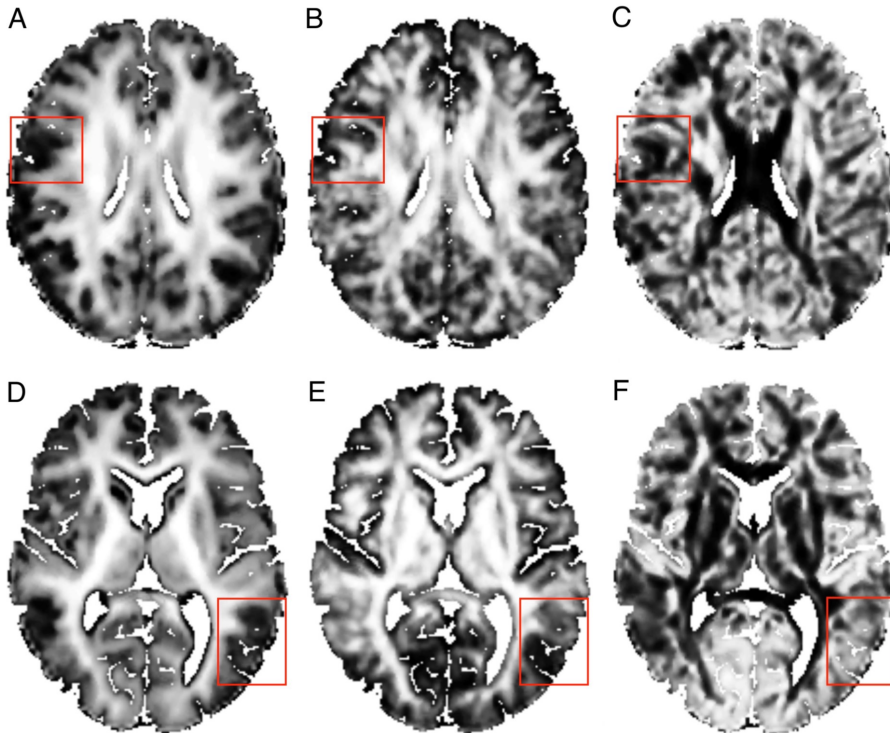


Figure 3.6: Comparison of the visibility of epilepsy on different metrics in two patients. The figure illustrates the comparison of MK, KFA and  $CM_{\text{contralateral}}$  for FCD type II between two patients: 2141300 and 2301188. The 1. row (A, B, C) corresponds to patient 2141300, while the 2. row (D, E, F) corresponds to patient 2301188. Within each row, the 1. column (A, D) represents MK, the 2. column (B, E) represents KFA, and the 3. column (C, F) represents a combined metric derived as the mean of individual CCA analyses in patients with FCD type II as listed in Table 3.7. The red square in each image roughly indicates the region where we observe the manifestation of epilepsy. The Figure demonstrates that the lesion is prominently visible in the combined metric for both patients, while the changes are more pronounced on the MK for patient 2141300, they are more conspicuous on the KFA for patient 2301188. All the pictures shown are after increasing the contrast using histogram equalization

To test the hypothesis in a similar way, univariate analysis was carried out for the control group. Similarly, as for the experimental group, the results of the correlation coefficients  $r$  are shown in Table 3.17, the distributions of correlations are shown using boxplots in Figure 3.8, and the bar plot with medians with designated confidence intervals is displayed in Figure 3.9.

Using the Mann-Whitney U test, we assessed the significance of differences in correlation coefficients  $r$  for each diffusion metric. In the overall analysis of all epilepsy patients, significant differences were observed for all diffusion parameters except FA, which still had a relatively low  $p$  value of 0.088. For patients with FCD type I, the MK metric performed best with a  $p$  value of 0.177, indicating that MK has the highest potential for identifying lesions in this type of epilepsy. Notably, for patients with FCD type I, we can confirm with 95% confidence that DTI FA and MD do not show significant differences in the contralateral analysis compared with the control group. In patients with FCD type II, MK had the least confidence in contralateral differences, with a  $p$ -value of 0.115. On the contrary, we found highly significant differences for MD between groups with a  $p$ -value  $< 0.001$ . Regarding the new combined metrics, the best results were observed in patients with FCD type II, particularly for the FCD-specific  $CM_{\text{contralateral}}$ , which had a  $p$ -value of 0.006. For patients with FCD type I, the new combined metrics did not demonstrate a clear advantage due to the high variability observed. All obtained  $p$ -values are listed in Table 3.16 and can also be compared using the bar plot in Figure 3.7.

Metric	All patients	FCD I	FCD II
T1	0.393	0.571	1.000
MD	0.013	0.950	$< 0.001$
FA	0.088	0.950	0.052
MK	0.018	0.177	0.115
KFA	0.030	0.489	0.019
$CM_{\text{voxelwise}}$	0.018	0.343	0.052
$CM_{\text{contralateral}}$	0.022	0.950	0.006
$CM_{\text{contralateral}}$ , (FA & MK only)	0.018	0.177	0.115
$CM_{\text{contralateral}}$ , (KFA & MK only)	0.030	0.489	0.019

Table 3.16: Significance of differences ( $p$ -values) in correlation coefficient  $r$  between experimental and control groups using Mann-Whitney U Test. A smaller  $p$ -value signifies a higher level of confidence in the distinction between the experimental and control groups concerning correlation  $r$  values derived from the contralateral comparison analysis

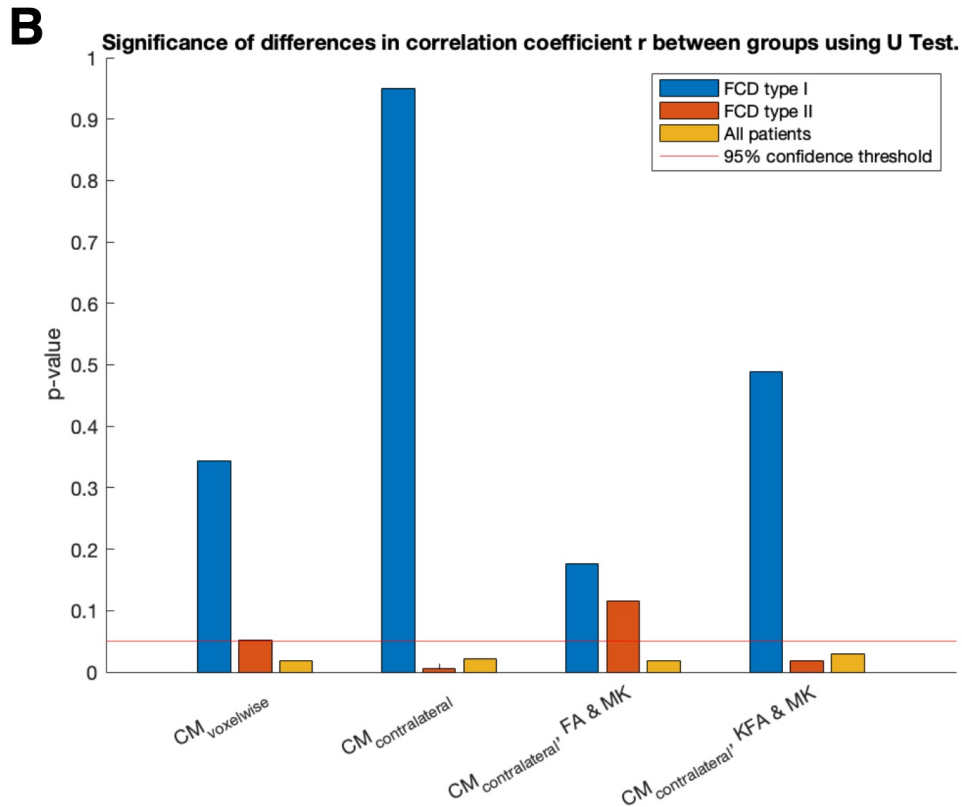
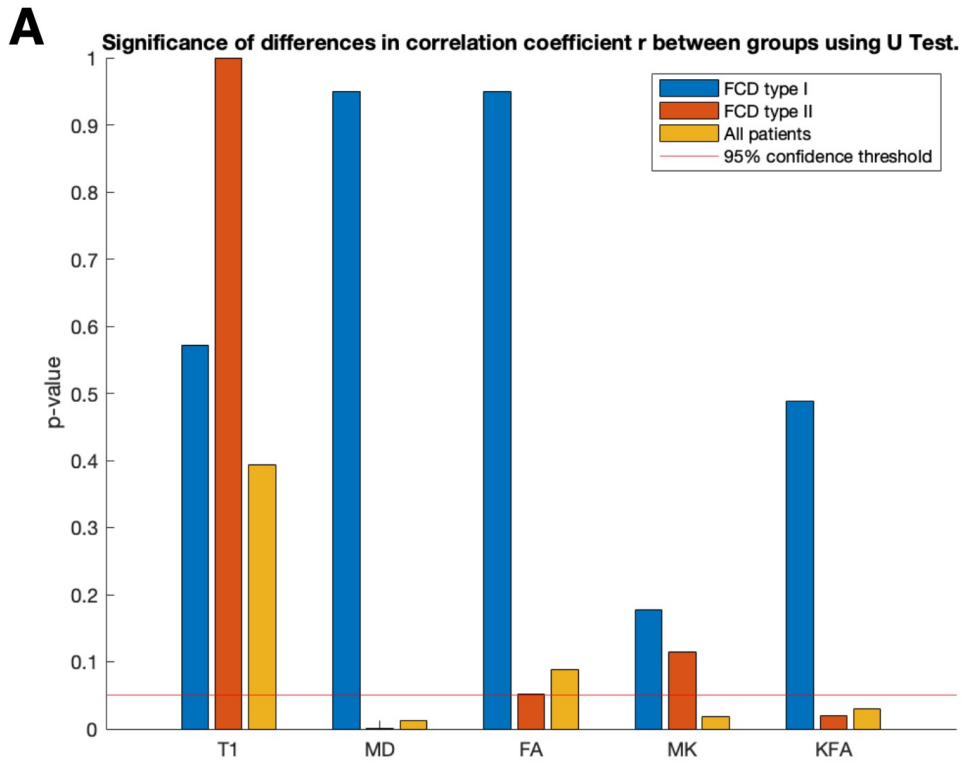


Figure 3.7: Plot depicting the significance in the distributional disparity of correlation coefficient  $r$  between experimental and control groups across various diffusion metrics, illustrated corresponding  $p$ -values from the U-test. (A) contains  $p$ -values for common metrics, (B) shows the newly created combined metrics from Sections 3.1 and 3.2.1. A smaller  $p$ -value signifies a higher level of confidence in the distinction between the experimental and control groups concerning correlation  $r$  values derived from the contralateral comparison analysis

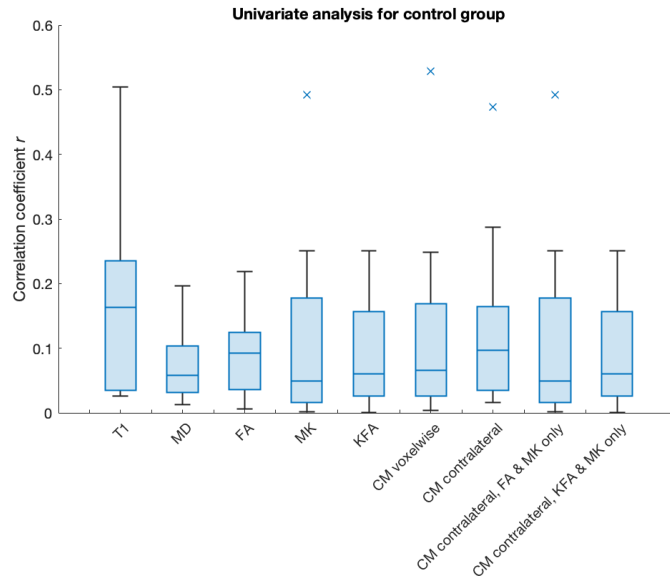


Figure 3.8: Box plots: Univariate analysis of the control group. A higher value of the correlation coefficient  $r$  indicates a greater practical discrepancy between the contralateral regions

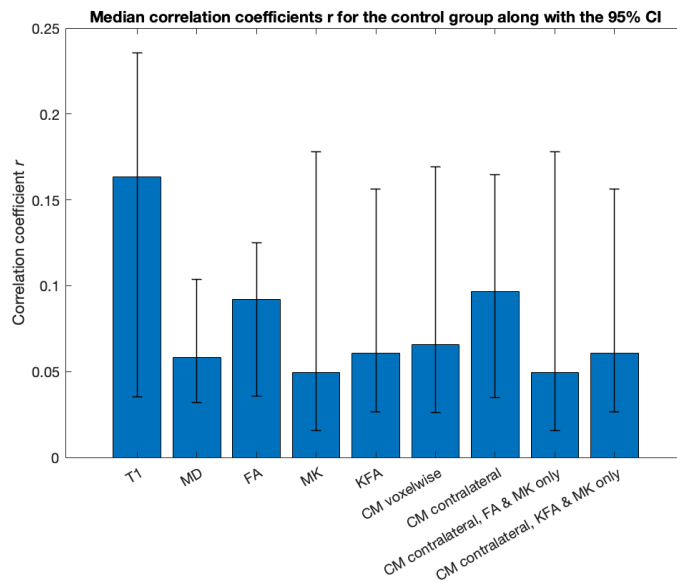


Figure 3.9: Bar plots: The medians of correlation coefficients  $r$  for the control group, along with their respective 95% confidence intervals (CI). A higher value of the correlation coefficient  $r$  indicates a greater practical discrepancy between the contralateral regions

Patients	Metrics								
	T1	MD	FA	MK	KFA	CM <sub>voxelwise</sub>	CM <sub>contralat.</sub>	CM <sub>contralat.</sub> FA & MK only	CM <sub>contralat.</sub> KFA & MK only
C14_1706135	0.4580	0.0775	0.1149	0.0021	0.0370	0.0261	0.0967	0.0021	0.0370
C15_2075044	0.2356	0.0126	0.0922	0.1779	0.0273	0.1691	0.1645	0.1779	0.0273
C16_2100410	0.5040	0.0727	0.2183	0.4923	0.2224	0.5283	0.4732	0.4923	0.2224
C17_2133603	0.1210	0.1263	0.0355	0.0246	0.0265	0.0396	0.0806	0.0246	0.0265
C18_2135840	0.0353	0.0320	0.0490	0.0157	0.0607	0.0041	0.1303	0.0157	0.0607
C19_2141300	0.1041	0.0365	0.0302	0.0296	0.0198	0.0294	0.0295	0.0296	0.0198
C20_2212090	0.2191	0.1037	0.0416	0.0495	0.0877	0.0657	0.0987	0.0495	0.0877
C21_2218031	0.0259	0.0188	0.0059	0.0022	0.0008	0.0046	0.0155	0.0022	0.0008
C22_2252569	0.1636	0.0540	0.1865	0.1558	0.1564	0.1415	0.0602	0.1558	0.1564
C23_2258839	0.1923	0.1964	0.1079	0.2509	0.2512	0.2482	0.2877	0.2509	0.2512
C24_2301188	0.0286	0.0583	0.1249	0.1429	0.1308	0.1297	0.0347	0.1429	0.1308

Table 3.17: Correlation coefficients  $r$  for each metric across control group patients. A higher value of the correlation coefficient  $r$  indicates a greater practical discrepancy between the contralateral regions

## 4. Discussion

The primary motivation of this study is to enhance the effectiveness and safety of brain resection in pharmaco-resistant epilepsy patients indicated for epileptology. An essential step in this process is a high-quality preoperative diagnosis to precisely identify the lesion for resection. Various examinations, such as EEG, PET, and MRI, are performed for this purpose. However, these methods often yield different boundaries for the affected region. For example, MRI often shows the lesion to be smaller or less noticeable than it is, which can be difficult to detect without the expertise of a highly trained radiologist, which is quite common in FCD type I.[5]

Diffusion MRI, which is a non-invasive examination, has the potential to reduce the above issues and, as a result, increase diagnostic efficiency. Therefore, in this study, the goal was to analyze the manifestations of the lesions on diffusion metrics, which can provide new information that can be used in the future when planning surgeries.

### 4.1 Statistical Analysis: Voxelwise and Contralateral Regions Comparison

To statistically assess the significance of diffusion metrics in epilepsy, a voxelwise comparison was conducted to analyze the specificity of affected voxel distribution compared to healthy one, irrespective of the anatomical brain region. This method is statistically advantageous because it involves a large number of voxels, even with a small patient sample. However, the practical application of these results is limited. Our findings indicate that the distributions of healthy and affected voxels are statistically significantly different for both FCD type I and FCD type II. Despite this, there is considerable overlap, as the intensities of lesioned voxels are also present in many healthy brain regions.

This issue is addressed through contralateral comparison analysis, comparing the affected region with the contralateral region within each patient. The contralateral analysis results provide more practical insights for radiologists in preoperative diagnosis, summarizing the extent and percentage of patients in which these regional distributions differ. However, a larger patient sample is needed for high-quality contralateral analysis to statistically confirm that the observed differences are specifically associated with epilepsy and not due to physiological asymmetry. For instance, in our study, it was not possible to conclusively determine significant contralateral differences for patients with FCD type I due to their heterogeneous diffusion metrics and smaller differences between healthy and pathological tissues, such as the absence of dysmorphic neurons and balloon cells, which are typical in FCD type II.[5]

Both analysis methods have several limitations. The first limitation is that the experimental group comprises a large number of pediatric images, while the control group consists entirely of adult patients. This discrepancy may affect the quality of normalization using the MNI template, which is based on adult brains and may not account for age-related features in the context of epilepsy

and brain development. Although the literature suggests that diffusion MRIs do not significantly differ with age after one year of postnatal life, but this claim was not tested in our study.[10]

The second significant limitation is the small sample size (4), which prevents us from examining the dependence of diffuse differences on specific anatomical regions of the brain. Therefore, the results should be interpreted with caution, especially when making statements about particular brain regions.

## 4.2 Univariate and Multivariate Contralateral Regions Comparison

In the literature on the use of DKI metrics in patients with epilepsy, each metric is often analyzed individually, or univariately. Since MRI scans generate three-dimensional images with a high number of slices, it is challenging for radiologists to analyze multiple metrics within a single image. Additionally, since computer processing can handle multidimensional data without limitations, treating the four diffusion metrics as a four-dimensional space rather than considering each metric individually may enhance the accuracy and effectiveness of classification. Through our analysis, we've identified a significant advantage in utilising multivariate techniques. Specifically, it enables us to develop combined metrics that enhance the detection of abnormalities by aggregating various diffusion parameters applicable to a specific disease.

Another important finding is that diffusion parameters, which do not have considerable contralateral differences in univariate analysis, may be decisive when considered together with other metrics. These aspects confirm the advantages of utilising a multivariate approach in preoperative diagnosis. Such a method reveals nuances that would otherwise remain covered when analyzing individual metrics in isolation. However, it requires an effective computer processing technique capable not only of accurately identifying abnormalities in the multidimensional space of diffusion parameters but also of effectively reducing dimensionality for subsequent assessment by radiologists.

It's important to highlight that while multivariate analysis is highly effective, it is a significantly more complex technique than univariate analysis. In this study, we used exclusively CCA, which is a linear method, so we are looking for a linear subspace in which the correlation (description of the dissimilarity in our case) is maximum. It is possible that the differences between affected regions can be more accurately described using nonlinear subspaces, which is a much more difficult problem both in finding such dependencies and in interpreting them. A logical continuation of CCA in subsequent works may be (Kernel Canonical Correlation Analysis) KCCA, which is a nonlinear analogue of this technique.

## 4.3 Contralateral Region Selection

In this study, we often searched for the region contralateral to the lesion identified by the radiologist. To select a method for discovering the contralateral region, we considered several options: mirroring in the MNI, manual designation of the contralateral region by a radiologist, and using an anatomical atlas. Several

primary experiments were conducted, which consisted of a qualitative comparison of selected contralateral regions by the radiologist and the mirroring method in the MNI. As a result, it turned out that both methods qualitatively carry, in most cases, similar information about the distribution of intensities in the contralateral regions. One example is indicated in Figure 4.1, where we can observe that both the contralateral region selected by the radiologist and the region selected by the automatic mirroring method in the MNI have similar distributions, both different from the lesion. Based on the data obtained and the fact that the use of an atlas as well as manual designation are more expensive methods, it was decided to select the contralateral regions by mirroring in the MNI space. As a result, we can observe that with the help of this simple method, it was possible to obtain reliable results regarding the manifestation of epilepsy on diffusion MRI. However, it is also worth remembering that in our study, in patients with FCD type I, it was not possible to confirm significant contralateral differences unrelated to physiological brain asymmetry, which may also be due to the weaknesses of the selected technique and its unsuitability for this type of FCD. Additional experiments on a larger number of patients are needed to evaluate this factor.

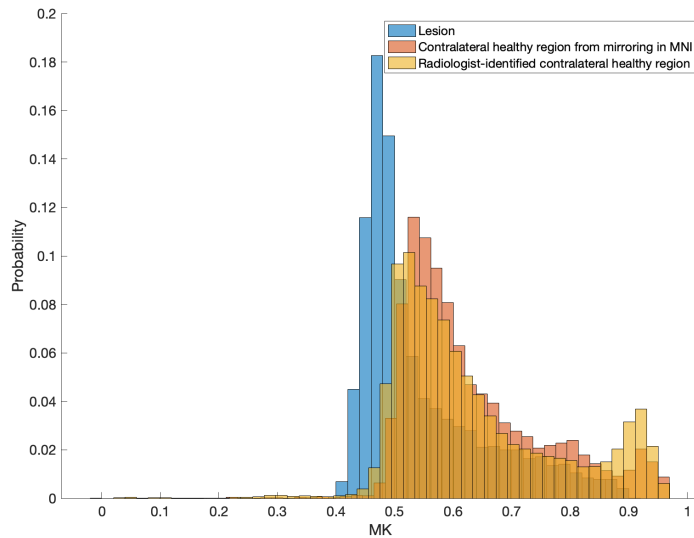


Figure 4.1: Differences in the distributions of healthy contralateral areas with different methods of obtaining them using the example of patient 2141300

## 4.4 Application in Presurgical Diagnosis

On structural MRIs, the affected region is often seen smaller than it is, so an optimistic result is if on DKI metrics the abnormality is visible not only within the boundaries designated by the radiologist on the structural T1 image but also beyond them. This result was obtained for patient 2252569, which is illustrated in Figure 4.2. However, it is worth noting that to date there is no reliable information about how the boundaries of diffuse MRI correlate with the actual boundaries of the affected region, which must be eliminated to stop the seizures.

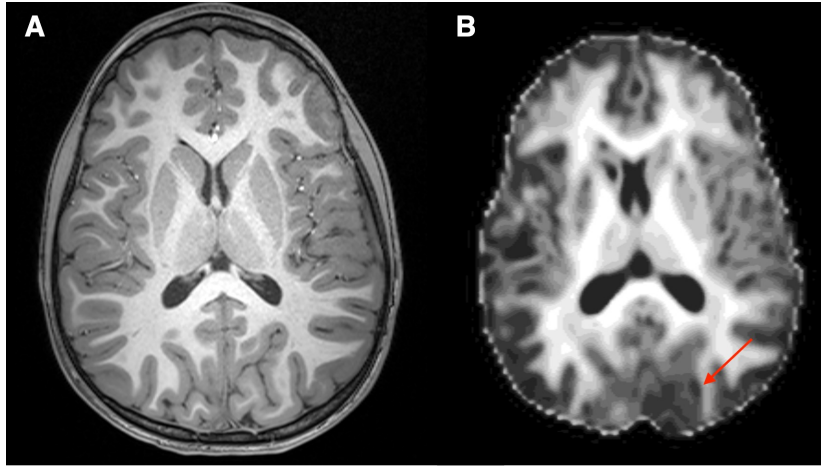


Figure 4.2: Detection of abnormalities in DKI metric beyond the designated lesion border identified using a T1 structural image. (A) Negative T1 image, (B) MK with the resulting contralateral abnormality (highlighted by a red arrow) extending from the identified lesion

## 4.5 Advanced Image Processing Techniques

### 4.5.1 Asymmetry Index

Unlike structural MRI, DKI metrics showed contralateral differences between lesion and healthy regions, indicating the importance of examining DKI metrics for asymmetry along the sagittal plane. This method is similar to the search for hypometabolic regions in PET images. At Motol University Hospital, technology for calculating the anatomical region asymmetry index is used to simplify this analysis.[27] We have attempted to apply this technology to DKI with varying success. In some instances, the method failed to detect asymmetry even when it was visually apparent, suggesting that adjustments to the methods and settings for diffuse MRI are necessary. This adjustment could be a focus for future research to aid radiologists in detecting abnormal asymmetry more efficiently. An example of successful use of the asymmetry index is shown for patient 2252569 in Figure 4.3.

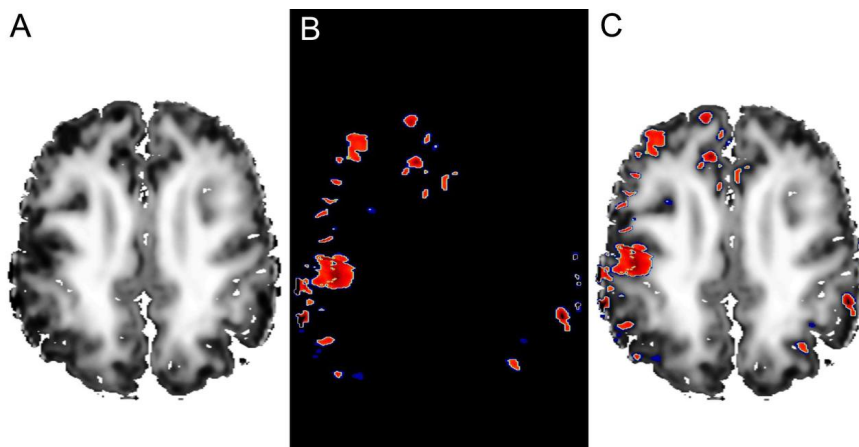


Figure 4.3: Application of the asymmetry index on DKI images. (A) Enhanced contrast displaying the MK, (B) Segmentation result based on the asymmetry index calculation [27], and (C) Combined image showing the segmentation results on the MK

### 4.5.2 Artificial Intelligence

In recent years, the application of artificial intelligence (AI) in medical imaging analysis has shown remarkable potential. The literature documents the successful creation of classifiers based on diffusion MRI. Notably, the integration of the diffusion metrics has been demonstrated to significantly improve classifier performance and coincides with the results of multivariate analysis in our study.[22].

Among the various classifiers, those utilizing tensors directly, specifically the diffusion and kurtosis tensors, have yielded superior results. The kurtosis tensor-based classification, in particular, has achieved outstanding accuracy, with an area under the curve (AUC) of 0.99, outperforming diffusion tensor imaging (DTI) which had an AUC of 0.96.[23] This indicates that the kurtosis tensor is highly effective in subtle differences in diffusion that may not be apparent in DTI.

Despite the demonstrated accuracy, interpreting the results from multidimensional classifiers poses a significant challenge.[28] The high dimensionality of tensor data complicates the extraction of clinically meaningful information. One potential solution to this issue is the application of dimensionality reduction techniques. Methods such as CCA or t-distributed stochastic neighbour embedding (t-SNE) can reduce the complexity of the data, making it more interpretable for the radiologist.

Another approach to using machine learning in tensor spaces is to support radiologists by providing a classification solution as new information, rather than offering a complete description of existing metrics as the reason for that choice. Segmentation algorithms can highlight potentially affected regions in medical images, but the basis for these decisions may not always be clear. Radiologists can use these algorithm-identified regions as a guide, allowing them to focus on areas flagged by diffusion MRI and perform further investigations, such as EEGs, to confirm the findings.

In conclusion, while the tensor-based approach in AI has demonstrated superior accuracy in medical imaging analysis, the complexity of high-dimensional data poses interpretative challenges, necessitating dimensionality reduction techniques like CCA and t-SNE to enhance clinical interpretability. Moreover, the role of AI should be seen as a supporting tool for radiologists rather than a stand-alone diagnostic solution. By highlighting potential lesions using segmentation algorithms, AI can guide radiologists to regions that require further investigation, thereby combining advanced computational techniques with expert clinical judgment. This synergistic approach ensures that artificial intelligence results are effectively used in clinical practice, ultimately improving diagnostic accuracy and surgical outcomes.

## 4.6 Future Work

In summary, many aspects of using DKI in preoperative diagnosis remain unclear. For instance, the correlation between the obtained images and histology has not been investigated, and the importance of diffusion information in planning resections is still uncertain. Our study yielded inconclusive results for patients with FCD type I, underscoring the need for further research with a larger patient cohort.

It is important to highlight that this study focused on MRI-positive patients, where lesions were detected on structural scans like T1. Future research extending to MRI-negative patients could provide additional insights, as diffusion MRI techniques may be particularly more valuable in those cases.

This work is innovative in its use of multidimensional statistics, although it employed only a linear method like CCA. Expanding the analysis to include nonlinear methods and directional statistics could provide new insights into the relationships between diffusion metrics in multidimensional space for different FCD types.

## 5. Conclusion

In conclusion, our study reveals statistically significant disparities in DKI metrics among patients diagnosed with both FCD types I and II, particularly in those identified as MRI-positive based on structural T1 imaging. Notably, the practical significance of these differences is more pronounced in FCD type II patients, contrasting with a lack of conclusive evidence in some cases of FCD type I.

An innovative aspect of our research lies in the utilization of multivariate statistical analysis, which allowed for a comprehensive examination of four diffusion metrics (MD, FA, MK, KFA) concurrently. This approach facilitated the development of novel combined metrics that integrate these parameters.

When comparing derived metrics, one stands out, especially for patients with FCD type II. We propose using a combined metric  $CM_{\text{contralateral}}$  derived from contralateral analysis exclusively for this FCD type:

$$CM_{\text{contralateral}} = -0.2608 \cdot MD - 0.3698 \cdot FA + 0.6212 \cdot MK - 0.4401 \cdot KFA \quad (5.1)$$

This approach enhances the sensitivity of lesion detection specifically for patients with FCD type II.



# Bibliography

1. CHEN, Zhibin; BRODIE, Martin J.; DING, Ding; KWAN, Patrick. Editorial: Epidemiology of epilepsy and seizures. *Frontiers in Epidemiology* [online]. 2023, vol. 3 [visited on 2024-05-15]. ISSN 2674-1199. Available from DOI: 10.3389/fepid.2023.1273163. Publisher: Frontiers.
2. *Epilepsy and Seizures — National Institute of Neurological Disorders and Stroke* [online]. [N.d.]. [visited on 2024-05-15]. Available from: <https://www.ninds.nih.gov/health-information/disorders/epilepsy-and-seizures>.
3. *Epilepsy* [online]. [N.d.]. [visited on 2024-05-15]. Available from: <https://www.who.int/news-room/fact-sheets/detail/epilepsy>.
4. BROMFIELD, Edward B.; CAVAZOS, José E.; SIRVEN, Joseph I. Epilepsy Surgery. In: *An Introduction to Epilepsy [Internet]* [online]. American Epilepsy Society, 2006 [visited on 2024-05-15]. Available from: <https://www.ncbi.nlm.nih.gov/books/NBK2514/>.
5. KABAT, Joanna; KRÓL, Przemysław. Focal cortical dysplasia – review. *Polish Journal of Radiology* [online]. 2012, vol. 77, no. 2, pp. 35–43 [visited on 2024-05-15]. ISSN 1733-134X. Available from: <https://www.ncbi.nlm.nih.gov/pmc/articles/PMC3403799/>.
6. KIM, Dong Wook; KIM, Sunghun; PARK, Sung-Hye; CHUNG, Chun-Kee; LEE, Sang Kun. Comparison of MRI features and surgical outcome among the subtypes of focal cortical dysplasia. *Seizure* [online]. 2012, vol. 21, no. 10, pp. 789–794 [visited on 2024-05-15]. ISSN 1059-1311. Available from DOI: 10.1016/j.seizure.2012.09.006.
7. CHANG, Won Seok; NAKAJIMA, Midori; OCHI, Ayako; WIDJAJA, Elysa; RUTKA, James T.; YAU, Ivanna; BABA, Shiro; OTSUBO, Hiroshi. Detection of epileptogenic focus using advanced dynamic statistical parametric mapping with magnetoencephalography in a patient with MRI-negative focal cortical dysplasia type IIB. *Journal of Neurosurgery: Pediatrics* [online]. 2019, vol. 25, no. 1, pp. 78–82 [visited on 2024-05-15]. ISSN 1933-0715, ISSN 1933-0707. Available from DOI: 10.3171/2019.7.PEDS1948. Publisher: American Association of Neurological Surgeons Section: Journal of Neurosurgery: Pediatrics.
8. LE BIHAN, Denis. Diffusion MRI: what water tells us about the brain. *EMBO Molecular Medicine* [online]. 2014, vol. 6, no. 5, pp. 569–573 [visited on 2024-05-16]. ISSN 1757-4676. Available from DOI: 10.1002/emmm.201404055.
9. O'DONNELL, Lauren J.; WESTIN, Carl-Fredrik. An introduction to diffusion tensor image analysis. *Neurosurgery clinics of North America* [online]. 2011, vol. 22, no. 2, pp. 185–viii [visited on 2024-05-20]. ISSN 1042-3680. Available from DOI: 10.1016/j.nec.2010.12.004.

10. VARGOVA, L.; HOMOLA, A.; CICANIC, M.; KUNCOVA, K.; KRSEK, P.; MARUSIC, P.; SYKOVA, E.; ZAMECNIK, J. The diffusion parameters of the extracellular space are altered in focal cortical dysplasias. *Neuroscience Letters* [online]. 2011, vol. 499, no. 1, pp. 19–23 [visited on 2024-05-01]. ISSN 03043940. Available from DOI: 10.1016/j.neulet.2011.05.023.
11. LEITE, Claudia; CASTILLO, Mauricio. *Diffusion Weighted and Diffusion Tensor Imaging: A Clinical Guide* [online]. New York, UNITED STATES: Thieme Medical Publishers, Incorporated, 2016 [visited on 2024-05-11]. ISBN 978-1-62623-020-0. Available from: <http://ebookcentral.proquest.com/lib/techlib-ebooks/detail.action?docID=4543354>.
12. *MRI instrumentation and safety: magnetic field gradients — e-MRI* [online]. [N.d.]. [visited on 2024-05-11]. Available from: <https://www.imaios.com/en/e-mri/mri-instrumentation-and-mri-safety/magnetic-field-gradients>.
13. KOAY, Cheng Guan; ÖZARSLAN, Evren. Conceptual Foundations of Diffusion in Magnetic Resonance. *Concepts in magnetic resonance. Part A, Bridging education and research* [online]. 2013, vol. 42, no. 4, pp. 116–129 [visited on 2024-05-23]. ISSN 1546-6086. Available from DOI: 10.1002/cmr.a.21269.
14. BASSER, Peter J.; JONES, Derek K. Diffusion-tensor MRI: theory, experimental design and data analysis – a technical review. *NMR in Biomedicine* [online]. 2002, vol. 15, no. 7-8, pp. 456–467 [visited on 2024-05-13]. ISSN 1099-1492. Available from DOI: 10.1002/nbm.783.
15. GLENN, G. Russell; HELPERN, Joseph A; TABESH, Ali; JENSEN, Jens H. Quantitative Assessment of Diffusional Kurtosis Anisotropy. *NMR in biomedicine* [online]. 2015, vol. 28, no. 4, pp. 448–459 [visited on 2024-05-20]. ISSN 0952-3480. Available from DOI: 10.1002/nbm.3271.
16. *Magnetism* [online]. [N.d.]. [visited on 2024-05-20]. Available from: <http://mriquestions.com/diffusion-kurtosis.html>.
17. WU, Ed X.; CHEUNG, Matthew M. MR diffusion kurtosis imaging for neural tissue characterization. *NMR in Biomedicine* [online]. 2010, vol. 23, no. 7, pp. 836–848 [visited on 2024-05-11]. ISSN 1099-1492. Available from DOI: 10.1002/nbm.1506.
18. HANSEN, B. An Introduction to Kurtosis Fractional Anisotropy. *AJNR: American Journal of Neuroradiology* [online]. 2019, vol. 40, no. 10, pp. 1638–1641 [visited on 2024-05-20]. ISSN 0195-6108. Available from DOI: 10.3174/ajnr.A6235.
19. MUHLHOFER, Wolfgang; TAN, Yee-Leng; MUELLER, Susanne G.; KNOWLTON, Robert. MRI-negative temporal lobe epilepsy—What do we know? *Epilepsia* [online]. 2017, vol. 58, no. 5, pp. 727–742 [visited on 2024-05-20]. ISSN 1528-1167. Available from DOI: 10.1111/epi.13699.

20. BARTOŇOVÁ, Michaela; BARTOŇ, Marek; ŘÍHA, Pavel; VOJTÍŠEK, Lubomír; BRÁZDIL, Milan; REKTOR, Ivan. The benefit of the diffusion kurtosis imaging in presurgical evaluation in patients with focal MR-negative epilepsy. *Scientific Reports* [online]. 2021, vol. 11, p. 14208 [visited on 2024-05-20]. ISSN 2045-2322. Available from DOI: 10.1038/s41598-021-92804-w.
21. GENNARI, Antonio Giulio; CSERPAN, Dorottya; STEFANOS-YAKOUB, Ilona; KOTTKE, Raimund; O'GORMAN TUURA, Ruth; RAMANTANI, Georgia. Diffusion tensor imaging discriminates focal cortical dysplasia from normal brain parenchyma and differentiates between focal cortical dysplasia types. *Insights into Imaging* [online]. 2023, vol. 14, no. 1, p. 36 [visited on 2024-05-20]. ISSN 1869-4101. Available from DOI: 10.1186/s13244-023-01368-y.
22. HUANG, Jianjun; XU, Jiahui; KANG, Li; ZHANG, Tijiang. Identifying Epilepsy Based on Deep Learning Using DKI Images. *Frontiers in Human Neuroscience* [online]. 2020, vol. 14, p. 590815 [visited on 2024-05-01]. ISSN 1662-5161. Available from DOI: 10.3389/fnhum.2020.590815.
23. KANG, Li; CHEN, Jin; HUANG, Jianjun; ZHANG, Tijiang; XU, Jiahui. Identifying epilepsy based on machine-learning technique with diffusion kurtosis tensor. *CNS Neuroscience & Therapeutics* [online]. 2021, vol. 28, no. 3, pp. 354–363 [visited on 2024-05-20]. ISSN 1755-5930. Available from DOI: 10.1111/cns.13773.
24. WINSTON, Gavin P. The potential role of novel diffusion imaging techniques in the understanding and treatment of epilepsy. *Quantitative Imaging in Medicine and Surgery* [online]. 2015, vol. 5, no. 2, pp. 279–287 [visited on 2024-05-20]. ISSN 2223-4292. Available from DOI: 10.3978/j.issn.2223-4292.2015.02.03.
25. GASER, Christian; DAHNK, Robert. *Computational Anatomy Toolbox for SPM* [online]. [N.d.]. [visited on 2024-04-16]. Available from: <https://neuro-jena.github.io/cat/>.
26. TOMCZAK, Ewa; TOMCZAK, Maciej. The need to report effect size estimates revisited. An overview of some recommended measures of effect size. *Biblioteka Akademii Wychowania Fizycznego w Poznaniu* [online]. 2014 [visited on 2024-04-16]. Available from: <https://www.wbc.poznan.pl/dlibra/publication/413565/edition/325867>.
27. MACKOVÁ, Kateřina. Assessment of hypometabolism in positron emission tomography [online]. 2021 [visited on 2024-05-23]. Available from: <https://dspace.cvut.cz/handle/10467/94432>. Publisher: Czech Technical University in Prague. Computing and Information Centre.
28. ADLER, Sophie; WAGSTYL, Konrad. *MELD Surface-based FCD Classifier* [online]. 2022. [visited on 2024-05-24]. Available from: [https://MELDProject.github.io//studies/MELD\\_FCD/](https://MELDProject.github.io//studies/MELD_FCD/).



# List of Figures

1.1	Illustrative MRI features in FCD patients. . . . .	6
1.2	Preoperative evaluation when preoperative axial T1-weighted image shows no visible abnormality. . . . .	7
1.3	Schematic illustration describing the propagation of diffusion in axons. Taken from [9] . . . . .	8
1.4	Simplified model describing coils in an MRI scanner. Taken from [12] . . . . .	8
1.5	A graph explaining what kurtosis means in the sense of normal distribution. Taken from [16] . . . . .	10
2.1	Diagram: Mirroring in MNI space . . . . .	17
2.2	Voxelwise analysis pipeline Diagram . . . . .	19
2.3	Visual representation of effect sizes contrasting correlation coefficients $r$ . . . . .	20
3.1	Histograms depicting voxelwise differences in the canonical components from the CCA . . . . .	24
3.2	Comparisons of correlation coefficients $r$ from the voxelwise analysis . . . . .	26
3.3	Distributions of correlation coefficients $r$ from multivariate analysis for the experimental and control groups . . . . .	29
3.4	Box plots: Univariate analysis of the experimental group . . . . .	35
3.5	Bar plots: The medians of correlation coefficients $r$ for the experimental group, along with their respective 95% confidence intervals (CI) . . . . .	36
3.6	Comparison of the visibility of epilepsy on different metrics in two patients . . . . .	38
3.7	Bar plot of $p$ -value significance from the U test: differences in correlation coefficients for each diffusion metric between the experimental and control groups . . . . .	40
3.8	Box plots: Univariate analysis of the control group. . . . .	41
3.9	Bar plots: The medians of correlation coefficients $r$ for the control group, along with their respective 95% confidence intervals (CI) . . . . .	41
4.1	Differences in the distributions of healthy contralateral areas with different methods of obtaining them . . . . .	45
4.2	Detection of abnormalities in DKI metric beyond the designated lesion border identified using a T1 structural image. . . . .	46
4.3	Application of the asymmetry index on DKI images . . . . .	46



# List of Tables

2.1	Patients of the control and experimental groups . . . . .	15
2.2	Configuration Settings for MNI Normalization . . . . .	17
3.1	Results of voxelwise CCA with 10-fold repetition in experimental group patients with all FCD types . . . . .	23
3.2	Results of voxelwise CCA with 10-fold repetition in experimental group patients with FCD type I . . . . .	25
3.3	Results of voxelwise CCA with 10-fold repetition in experimental group patients with FCD type II . . . . .	26
3.4	Results of voxelwise CCA with 10-fold repetition in control group patients. Coefficient $r$ indicates the degree of difference between distributions . . . . .	26
3.5	Results of multivariate analysis using CCA in all patients in the experimental group . . . . .	27
3.6	Results of multivariate analysis using CCA in patients with FCD type I in the experimental group . . . . .	28
3.7	Results of multivariate analysis using CCA in patients with FCD type II in the experimental group . . . . .	28
3.8	Results of multivariate analysis using CCA in control group patients	30
3.9	Results of contralateral multivariate analysis by CCA, using exclusively FA and MK metrics, in all patients in the experimental group . . . . .	31
3.10	Results of contralateral multivariate analysis by CCA, using exclusively FA and MK metrics, in patients with FCD type I in the experimental group . . . . .	31
3.11	Results of contralateral multivariate analysis by CCA, using exclusively FA and MK metrics, in patients with FCD type II in the experimental group . . . . .	31
3.12	Results of contralateral multivariate analysis by CCA, using exclusively KFA and MK metrics, in all patients in the experimental group . . . . .	32
3.13	Results of contralateral multivariate analysis by CCA, using exclusively KFA and MK metrics, in patients with FCD type I in the experimental group . . . . .	32
3.14	Results of contralateral multivariate analysis by CCA, using exclusively KFA and MK metrics, in patients with FCD type II in the experimental group . . . . .	33
3.15	Correlation coefficients $r$ for each metric across experimental group patients . . . . .	37
3.16	Significance ( $p$ -values) from the U-test: differences in correlation coefficients for each diffusion metric between the experimental and control groups . . . . .	39
3.17	Correlation coefficients $r$ for each metric across control group patients	42



# List of Abbreviations

<b>AI</b>	Artificial Intelligence
<b>AUC</b>	Area Under the Curve
<b>CCA</b>	Canonical Correlation Analysis
<b>CM</b>	Combined Metric
<b>CSF</b>	Cerebral Spinal Fluid
<b>DKI</b>	Diffusion Kurtosis Imaging
<b>DTI</b>	Diffusion Tensor Imaging
<b>DWI</b>	Diffusion-weighted Imaging
<b>EEG</b>	Electroencephalogram
<b>FA</b>	Fractional Anisotropy
<b>FCD</b>	Focal Cortical Dysplasia
<b>FLAIR</b>	Fluid Attenuated Inversion Recovery
<b>fMRI</b>	Functional Magnetic Resonance Imaging
<b>KCCA</b>	Kernel Canonical Correlation Analysis
<b>KFA</b>	Kurtosis Fractional Anisotropy
<b>MCD</b>	Malformation of Cortical Development
<b>MD</b>	Mean Diffusivity
<b>MEG</b>	Magnetoencephalography
<b>MK</b>	Mean Kurtosis
<b>MRI</b>	Magnetic Resonance Imaging
<b>PET</b>	Positron Emission Tomography
<b>t-SNE</b>	t-distributed Stochastic Neighbor Embedding
<b>SD</b>	Standard Deviation

